Mechanism and Kinetics of Methylating C_6–C_{12} Methylbenzenes with Methanol and DME in H-MFI Zeolites

Mykela DeLuca, Pavlo Kravchenko, Alexander Hoffman, David Hibbitts*

Department of Chemical Engineering, University of Florida, Gainesville, 32611

Abstract

This study uses periodic density functional theory (DFT) to determine the reaction mechanism and effects of reactant size for all 20 arene (C_6–C_{12}) methylation reactions using CH_3OH and CH_3OCH_3 as methylating agents in H-MFI zeolites. Reactant, product, and transition state structures were manually generated, optimized, and then systematically reoriented and reoptimized to sufficiently sample the potential energy surface and thus identify global minima and the most stable transition states which interconnect them. These systematic reorientations decreased energies by up to 50 kJ mol^{-1}, demonstrating their necessity when analyzing reaction pathways or adsorptive properties of zeolites. Benzene-DME methylation occurs via sequential pathways, consistent with prior reports, but is limited by surface methylation which is stabilized by co-adsorbed benzene via novel cooperativity between the channels and intersections within MFI. These co-adsorbate assisted surface methylations generally prevail over unassisted routes. Calculated free energy barriers and reaction energies suggest that both the sequential and concerted methylation mechanisms can generally occur, depending on the methylating agent and methylbenzene being reacted—there is no consensus mechanism for these homologous reactions. Intrinsic methylation barriers for step-wise reactions of benzene to hexamethylbenzene remain between 75–137 kJ mol^{-1} at conditions relevant to methanol-to-hydrocarbon (MTH) reactions where such arene species act as co-catalysts. Intrinsic methylation barriers are similar between CH_3OH and CH_3OCH_3 suggesting that both species are equally capable of interconverting between methylbenzene species. Additionally, these methylation barriers do not systematically increase as the number of methyl-substituents on the arene increases and the formation of higher methylated arenes is thermodynamically favorable. These barriers are significantly lower than those associated with alkene formation during the aromatic cycle, suggesting that aromatic species formed during MTH reactions either egress from the catalyst—depending on that zeolite's pore structure—or become trapped as extensively-substituted C_{10}–C_{12} species which can either isomerize to form olefins or ultimately create polyaromatic species that deactivate MTH catalysts.

1. Introduction

Brønsted-acid-catalyzed alkylation reactions are ubiquitous, occurring during alcohol dehydration,[1,2] alkene oligomerization,[3,4] and methanol-to-hydrocarbon (MTH) reactions.[5,6] Methanol does not directly couple to form C–C bonds during MTH reactions or does so at low rates.[5,7–9] Instead, zeolite surfaces, alkenes, and arenes are methylated by a combination of methanol (CH_3OH) and dimethyl ether (CH_3OCH_3), both present at MTH conditions. Alkenes can grow through repeated methylation reactions (reacting with surface methoxy species or directly with methylating agents such as CH_3OH and CH_3OCH_3). Larger C_{6+} alkenes can crack into C_2–C_4 alkenes which can desorb as products or re-alkylate in the alkene cycle, in which olefins are alkylated and crack to form other alkene species of varying lengths.[10–15] For example, three CH_3OH molecules may sequentially methylate propene to form hexene which could crack into two propene molecules; as such, this olefin-forming process can be "auto-catalytic" as alkenes are both co-catalysts and products of MTH. Alkenes may, instead of cracking, undergo hydride transfer reactions with other alkenes (to form alkanes and dienic compounds) or with methanol (to form alkanes, formaldehyde, and ultimately dienes) and then cyclize in mono- or bimolecular routes to ultimately form aromatic compounds (arenes).[16,17] These arenes can be methylated during MTH to form one of twelve distinct C_7–C_{12} methylbenzene species, shown in Fig. 1. Many of these methylbenzene species can undergo isomerization and dealkylation reactions to produce light alkene products that can egress from the zeolite crystal or join the alkene cycle; thus, these alkene products from methylbenzenes may be incorporated into other aromatic compounds, again leading to auto-catalytic behavior.[18–21] Therefore, understanding how these arene co-catalysts interconvert is key to understanding the larger MTH reaction network. Arene methylation, in addition to its role in MTH, is also important in the formation of toluene from benzene, toluene disproportionation to xylenes, and other transalkylation reactions.[22–25] Despite the ubiquity of arene methylation reactions in industrial processes, there are few studies contrasting arene methylation mechanisms with CH_3OH and CH_3OCH_3 and fewer studies elucidating methylation mechanisms across a wide range of methylbenzene reagents.

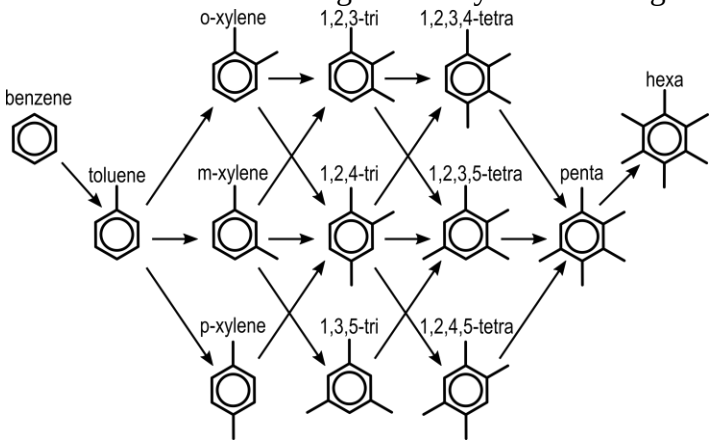

Figure 1. All possible methylation pathways of C_6–C_{12} methylbenzene species.

Brønsted-acid-catalyzed alkylation reactions occur via one of two distinct mechanisms[6,26–31]: a sequential mechanism (also known as the dissociative or indirect mechanism) or a concerted mechanism (also known as the associative or direct mechanism). In the sequential mechanism, the methylating agent first methylates the zeolite to form a surface methoxy species (CH_3–Z) preceding the methylation of an alcohol, alkene, or arene:

$$ROCH_3 + H\text{–}Z \rightarrow [ROH\cdots CH_3^+\cdots Z^-]^{\neq} \rightarrow ROH + CH_3\text{–}Z \quad (1)$$

$$C_6H_6 + CH_3\text{–}Z \rightarrow [C_6H_6\cdots CH_3^+\cdots Z^-]^{\neq} \rightarrow C_7H_8 + H\text{–}Z \quad (2)$$

In the concerted mecahnism, the methylating agent directly reacts with an alcohol, alkene, or arene:

$$ROCH_3 + C_6H_6 + H\text{–}Z \rightarrow [ROH\cdots CH_3^+\cdots C_6H_6 + Z^-]^{\neq} \rightarrow ROH + C_7H_8 + H\text{–}Z \quad (3)$$

Surface methoxy species are a reactive intermediate in the sequential pathway, but not the concerted pathway and their presence is commonly used to differentiate between these pathways. The purging of CH_3OCH_3-C_6H_6 after reaction in a pillared MFI framework zeolite (H-SPP, 358 K) followed by a subsequent heat treatment (423 K) and titration with H_2O formed CH_3OH in a 1:1 ratio with Al, suggesting high surface methoxy coverages.[28] Benzene and toluene d_6 DME/DME switching experiments demonstrate a 1:2:1 ratio of d_0:d_3:d_6 indicating rapid C−O bond breaking and formation at reaction conditions,[28] consistent with alkene methylation studies.[29] However, CH_3–Z species were not identified by FT-IR during the co-reaction of benzene and CH_3OH at 623 K at steady state—conditions that better represent those of MTH processes[27]—suggesting that the presence of an arene at reaction conditions may alter the amount of surface methoxy species formed. The absence, presence, or abundance of CH_3–Z, however, does not rule out either methylation mechanism. For instance, the absence or scarcity of CH_3–Z species can indicate that the concerted mechanism occurs (i.e., they are not formed) or that ring methylation consumes CH_3–Z too fast for them to accumulate to detectable levels. Similarly, high coverages of CH_3–Z species do not preclude the concerted mechanism from occurring, as CH_3–Z species may be unreactive spectators in arene methylation or react predominantly with oxygenate species.

The sequential and concerted mechanisms may also differ by the kinetic dependencies of the methylating agent (CH_3OR), the leaving group (ROH), and the species being methylated (alcohol, alkene, or arene). Kinetic studies (0.01 bar aromatic, 0.2–0.5 bar CH_3OCH_3, 0.01% conversion) of benzene (373 K), toluene (403 K), and xylene (473 K) methylation with CH_3OCH_3 have shown rates independent of CH_3OCH_3 pressure and linearly dependent on arene pressure.[28] Coupled zero-order effects of CH_3OCH_3 and first-order effects of arene reagents suggest that sequential alkylation pathways prevail and are limited by arene alkylation steps on surfaces covered by CH_3–Z species; however, co-adsorbate assisted surface methylation reactions have not been considered.[28] Density functional theory (DFT) calculations on a cluster of four T-atoms and ab initio molecular dynamic studies indicate concerted methylation barriers are > 30 kJ mol^{-1} lower than those of sequential methylation with CH_3OCH_3.[32,33] These theoretical data suggest that benzene methylation proceeds via concerted methylation;[28,29] however, cluster models fail to adequately model periodic zeolite catalysts and do not capture the critical dispersive interactions in zeolite pores that stabilize guest species.[34] There is an apparent disparity between computational studies and experimental studies regarding the coverage and role of CH_3–Z species and the route by which arenes are methylated.

Theoretical and experimental work have demonstrated that CH_3OCH_3 methylates alkenes and arenes at a faster rate than CH_3OH. CH_3OCH_3 methylates propene at a rate 2.5 times faster than CH_3OH in H-ZSM-5 (523 K, 0.02 bar propene, 0.025–0.075 bar CH_3OH or CH_3OCH_3).[11] DFT calculations on cluster models with four tetrahedral sites (T-sites) similarly predict that concerted methylation of both propene and toluene occur with lower barriers from CH_3OCH_3 during methylation rather than CH_3OH.[11] Computational and experimental studies generally agree that CH_3OCH_3 is the dominant methylation agent at typical arene methylation conditions (low conversions, 400–600K).[35–37] These comparisons between CH_3OH and CH_3OCH_3 are limited to methylations of C_6–C_8 arenes; larger, extensively substituted methylbenzene species, however, may crowd out CH_3OCH_3 molecules in favor of smaller CH_3OH, thereby limiting the effectiveness of CH_3OCH_3 during methylation.

Few studies investigate the effects of arene substitution on methylation barriers and preferred methylation mechanisms. DFT calculations on a 4 T-site cluster model predicted that concerted CH_3OH-arene methylation barriers were 191 kJ mol^{-1}, 174 kJ mol^{-1}, and 171 kJ mol^{-1} for toluene, 1,2,4,5-tetramethylbenzene, and hexamethylbenzene leading to the conclusion that methylation barriers decrease as the number of methyl substituents increases.[38] Conversely, rates of *ortho*- and *para*-xylene methylation (473 K, 0.01 bar xylene, 0.1% conversion, 0.68 bar CH_3OCH_3) in H-ZSM-5 were lower than those for benzene (373 K, 0.01 bar benzene, 0.1% conversion, 0.68 bar CH_3OCH_3); however, differences in temperature and the mass transport properties of these

reactants make direct comparisons more difficult.[28] A possible cause for the discrepancy between theoretical and experimental trends on the effects of methyl-substitution on arene methylation could be the lack of confinement effects—responsible for lowering the barriers for methylation of smaller arenes through stabilization effects and raising the barriers for methylation of larger arenes through repulsive interactions—in cluster calculations. Zeolite models with fully periodic boundary conditions can overcome the limitations of cluster calculations, but to our knowledge, arene methylation has not been investigated using fully periodic models.

Here, we use fully periodic density functional theory (DFT) calculations to investigate the methylation of all possible methylbenzene co-catalysts via the concerted and sequential mechanisms with methylating agents CH_3OH and CH_3OCH_3 in H-MFI. Systematic reorientations were performed on all states to sample the potential energy surface and identify the global minimum for each state, rather than local minima obtained from single optimizations. Sampling the potential energy surface using this method is crucial to obtain reliable results in ground-state theoretical zeolite studies, as energies decreased by up to 50 kJ mol^{-1} after systematically reorienting species. We also show that benzene methylation occurs via the sequential mechanism, consistent with experimental results and that the rate is limited by the formation of CH_3–Z, which occurs in the presence of adsorbed benzene. Co-localized arene species stabilize the surface methylation transition states through additional dispersive interactions, cooperating with the surrounding zeolite framework to stabilize these structures and providing insight into the unique reactivity of MFI as enabled by the joining of diverse channel and intersection environments. Stepwise methylation barriers of benzene to hexamethylbenzene, relevant to MTH reactions, indicate that these reactions are relatively facile and the formation of higher methylated species is thermodynamically favorable, suggesting that aromatic species formed during MTH reactions either escape zeolite domains or become trapped as C_{10}–C_{12} methylbenzene species which can co-catalyze olefin formation or lead to catalyst deactivation.

2. Methods

2.1 Computational Methods

DFT calculations were carried out using the Vienna ab initio simulation package (VASP)[39–42] in a fully periodic MFI unit cell. Planewaves were constructed using projector augmented-wave (PAW)[43,44] potentials with an energy cutoff of 400 eV. The Perdew-Burke-Ernzerhof (PBE) form of the generalized gradient approximation (GGA) was used to determine exchange and correlation energies.[45–47] The DFT-D3 method with Becke and Johnson damping accounted for dispersive interactions.[48–50] The Brillouin zone was sampled at the Γ-point for all calculations.[51]

The MFI structure was obtained from the IZA database[52] and annealed using ab initio molecular dynamics (AIMD) to generate a low-energy state for these DFT settings. The structure was heated from 200 K to 800 K over 3000 fs, held at 800 K for 3000 fs, then cooled over 15000 fs. During these AIMD studies, the wavefunction for each step was converged to within 10^{-4} eV and one atom was fixed to prevent bulk translation. The final structure obtained after annealing and optimizing is 23 kJ mol^{-1} more stable than the directly optimized IZA structure (Fig. S1, in the Supporting Information, SI). These calculations were done to ensure stability within the baseline framework and to prevent framework restructuring from altering calculated activation and reaction energies, as described in detail elsewhere.[53] All calculations were performed at the T11 tetrahedral site (T-site) in MFI, which gives access to both the straight channel and the channel intersection where arenes prefer to populate.

All reactant, product, and transition states were optimized in static DFT calculations until the maximum force on any atom was < 0.05 eV $Å^{-1}$. Wave functions were converged to within 10^{-6} eV and all forces were computed using a fast Fourier transform (FFT) grid with a cutoff twice the planewave cutoff. No atoms were constrained in any DFT optimization, pathway, or transition state calculations while the lattice parameters (a = 20.090 Å, b = 19.738 Å, c = 13.142 Å) and orthorhombic shape were fixed.

Minimum energy pathways were estimated using the nudged elastic band (NEB)[54,55] method. NEB calculations used 16 images and wavefunctions converged to 10^{-4} eV with an FFT grid 1.5 times the size of the plane-wave cutoff. The maximum force on each atom in all images were converged to < 0.5 eV $Å^{-1}$. This estimate of the minimum energy pathway was used to generate initial transition state structures and reaction modes for the Dimer method,[56] which optimizes a pair of structures to determine the local curvature of the potential energy surface until ultimately converging on a saddle point. The same convergence criteria were used for optimization and Dimer calculations (e.g., maximum forces on any atom < 0.05 eV $Å^{-1}$).

Frequencies were calculated for all reactant, product, and transition states using a fixed displacement method where the adsorbates (e.g., CH_3OH and benzene) and AlO_4 of the acid site are displaced while all other framework atoms are fixed. Low-frequency modes (< 60 cm^{-1}) were replaced with 60 cm^{-1}, similar to previous work,[57,58] because low frequencies are inaccurate and contribute significantly to vibrational entropy terms. These frequency calculations are used to determine temperature-corrected (373–673 K) enthalpies and free energies according to harmonic oscillator approximations for vibrational partition functions and ideal gas treatments of rotational and translational partition functions for bulk gas species.

2.2 Reorientations of reactant, product, and transition states

All DFT-optimized reactant, product, and transition states were systematically reoriented to increase the likelihood that global minima and optimum transition state structures were obtained via static (non-dynamic) DFT calculations. Species were first optimized from manually generated structures then reoriented based on the nature of the interaction between the adsorbate and the zeolite. Adsorbed species and transition states can interact with the zeolite in several ways: forming covalent bonds (e.g., CH_3–Z), forming H-bonds with Brønsted acid sites (e.g., CH_3OH*), or purely through nonspecific dispersive and electrostatic interactions (e.g., C_6H_6*, $C_7H_9^+$*). Three reorientations schemes are used here: acid site reorientations, internal reorientations, and spatial reorientations (Fig. 2 gives examples of all three).

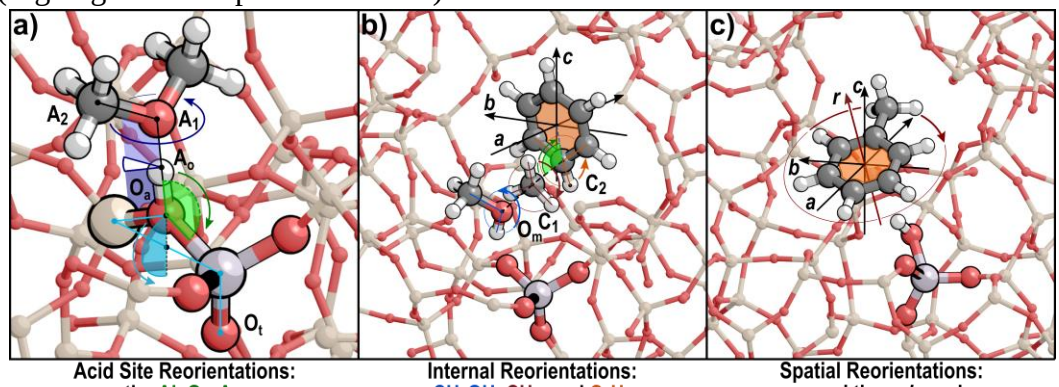

Figure 2. a) Three different acid site reorientations about the Al–O_a–A_1 angle (green), O_t–Al–Si–O_a angle (cyan), and O_t–O_a–A_1–A_2 angle (blue). **b)** Internal reorientations of the concerted transition state where CH_3OH (blue), CH_3 (brown), and C_6H_6 can be rotated about the O_m–C_1–C_2 angle formed between the leaving group, the adding CH_3, and the ring (orange). The angle of the ring can be altered relative to the adding CH_3 group by altering the CH_3–ring angle (green). **c)** Spatial reorientations of methylbenzene about the a-, b-, and c-axes of the unit cell and the axis perpendicular to the center of the ring (red). Larger versions of each image are available, for clarity, in the Supporting Information (Figs. S2–S4).

Adsorbates that covalently bind to the framework or form H-bonds with protonated Brønsted acid sites, such as adsorbed oxygenates and alkoxides, underwent acid site reorientations (e.g., CH_3OCH_3* in Fig. 2a). Structures

and acid sites are rotated by altering the dihedral angle formed between an O-atom of the acid site (O_t), the Al atom, the Si atom closest to the acid site, and the O to which the proton or alkoxide is bound (O_a) in O_t–Al–Si–O_a rotations. This motion effectively sweeps the adsorbed species around the acid site (Fig. 2a), as done previously for Brønsted acid site calculations.[59] The O_t–Al–Si–O_a angles were varied by 30° increments from 30°–330°. The angle between the Al atom, the O_a atom, and the adsorbate itself (A_1) can also be varied (Fig. 2a) to move the adsorbate above the acid site parallel to the Si–O_a–Al bridge, and this Al–O_a–A_1 angle was varied by –30°, –15°, 15°, and 30° from the initial optimized position. Finally, the dihedral angle between a T-site, the O_a atom, and two adsorbate atoms (A_1 and A_2) can be altered to spin the adsorbate around the O_a atom, as shown in Fig. 2a, the dihedral angles were varied by 30° increments from 30° to 330°.

Large transition state complexes associated with surface methylation, sequential methylation of the arene ring, or concerted methylation of the arene ring have multiple fragments that can rotate about breaking or nascent bonds. Concerted benzene methylation by CH_3OCH_3, for example, involves CH_3OH, methyl, and arene fragments (Fig. 2b) and these species can be reoriented relative to one another to isolate more stable transition state structures. The orientation of the ring relative to the attacking methyl group (ring-CH_3 angle) was altered so that the two species were co-planar. Furthermore, the ring was rotated about the axis of the oxygen of the CH_3OH group (O_m), the carbon of the attacking methyl species (C_1), and the carbon on the ring being attacked (C_2) so that the orientation of the ring changes without affecting the incipient bond of the transition state. Rotations about the O_m–C_1–C_2 axis were performed from 30° to 330° in 30° increments. This transition state complex, furthermore, can be rotated spatially as it interacts non-specifically with the zeolite framework and the deprotonated Brønsted acid site.

Adsorbate species that interact nonspecifically through a combination of dispersive and electrostatic interactions and without H-bonds to a protonated acid site were rotated in spatial reorientations (e.g., methylbenzene in Fig. 2c). Arenes were also rotated around the axis perpendicular to the ring (Fig. 2c). Species were rotated in 30° increments from 30° to 330° during these spatial reorientations; rotations resulting in collisions with the zeolite framework were discarded.

All reorientations described above are used as initial structures—they are not intended to determine torsional barriers or generate intramolecular potential energy surfaces; they are instead fully optimized in unconstrained calculations. As such, these reorientations serve to extensively seed a potential energy surface with multiple initial structures—each optimized—to potentially many local minima. These local minima are compared, and the minimum potential energy structures are used in further analysis; ideally these structures represent the global minimum state of that species.

3. Results and Discussion

3.1 Identifying the most stable orientations and locations of arene methylation species

The T11 T-site is used for all reactions in this study and is connected to four unique O-sites: O14 (straight channel), O16 (intersection), O24 (beneath intersection), and O25 (intersection) (see Fig. S5 in the Supporting Information). The O24 site is inaccessible for species larger than $-CH_3$ and, therefore, all other reactions were studied only at O14, O16, and O25, except for surface methylation, which was the modeled at all sites.

Systematic reorientations can find structures drastically lower in energy than their manually generated counterparts (Fig. 3). Three types of systematic reorientations were performed on guest species using static DFT calculations as appropriate: acid site, spatial, and internal reorientations. Each type of reorientation produced structures that were more stable than their manually generated counterparts. Fig. 3 shows a subset of the results of the reorientations performed for this study for CH_3OCH_3*, C_6H_6--CH_3OCH_3*, C_7H_8*, the transition state for surface methylation in the presence of benzene, the transition state for benzene methylation from a surface methoxy, and concerted benzene methylation on each accessible O site on T11.

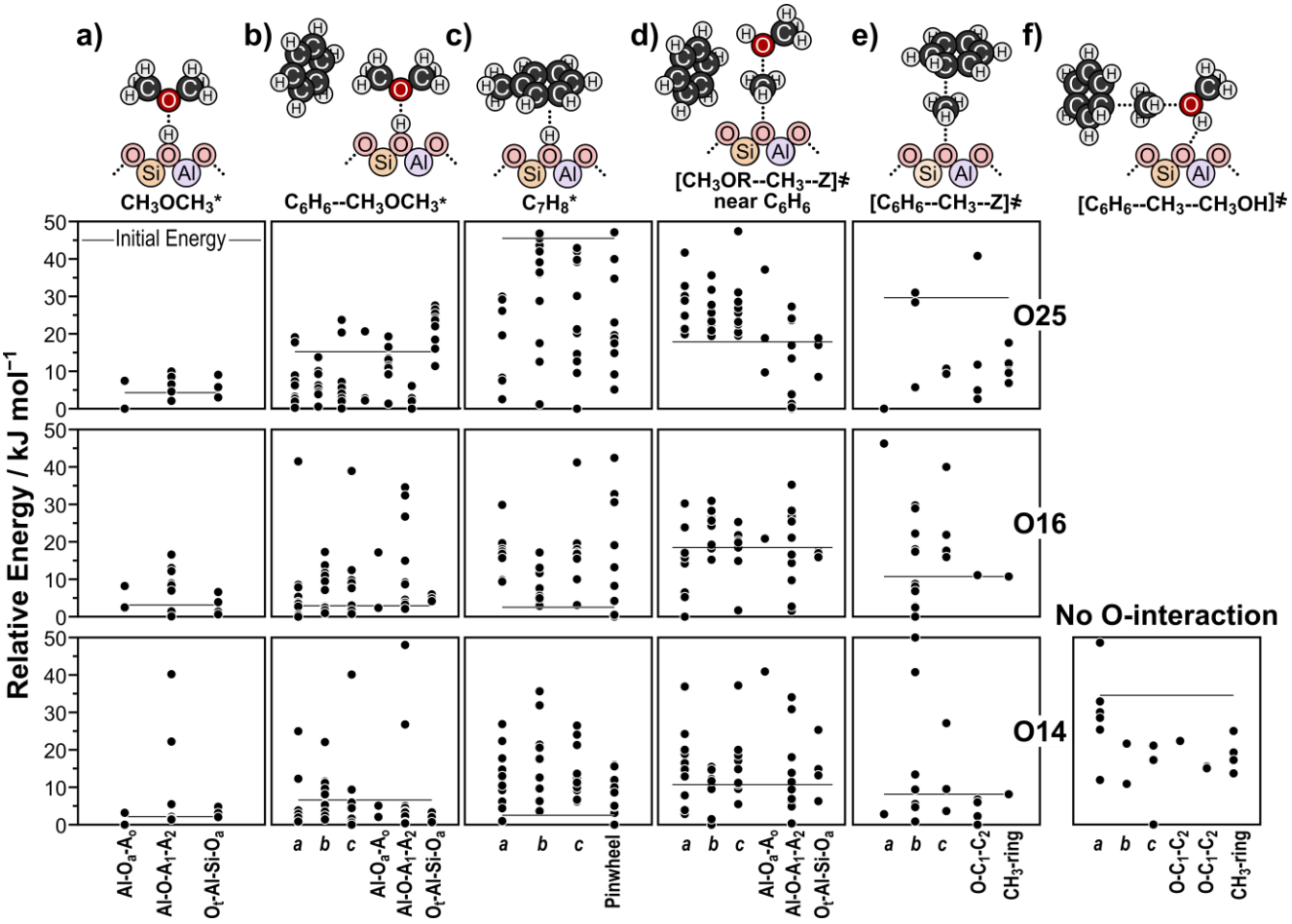

Figure 3. Energies of spatial reorientations (a-, b-, and c-axes), acid site reorientations (Al–O_a–A_o, A_l–O–A_1–A_2, and O_t–Al–Si–O_a), and internal reorientations (O–C_1–C_2 and CH_3-ring) performed on **a)** CH_3OCH_3*; **b)** C_6H_6--CH_3OCH_3*; **c)** C_7H_8*; **d)** the surface methylation transition state with CH_3OCH_3; **e)** the ring methylation transition state at O14, O16, and O25; and **f)** the concerted transition state, which does not covalently interact with an O-site, so reorientations are not O-dependent. All energies are relative to the most stable state at each respective O-site and reported in kJ mol^{-1}. The solid line represents the energy of the initial structure prior to reorientation.

Acid site reorientations were performed on adsorbates that covalently bind to the framework and those that form H-bonds to surface protons (e.g., CH_3OCH_3*) as described in Section 2.2. Structures were reoriented by altering the O_t–Al–Si–O_a, Al–O_a–A_1, and O_t–O_a–A_1–A_2 angles (Fig. 2a). These reorientations resulted in average energy decreases of 6.5 kJ mol^{-1}, 6.1 kJ mol^{-1}, and 11.3 kJ mol^{-1} compared to manually generated optimized structures for species relevant to benzene methylation. Fig. 3a shows reorientations of CH_3OCH_3 about O14, O16, and O25 resulting in energy decreases of ~6 kJ mol^{-1} at each acid site.

Spatial reorientations were performed on species that do not strongly interact with the Brønsted acid site (e.g., methylbenzene). The subset of structures relevant to benzene methylation were rotated about the a-, b-, and c-axes of the unit cell resulting in an average decrease in energy of 8.5, 7.2, and 8.4 kJ mol^{-1} respectively. Species with one or more methyl-substituents on the benzene ring (methylbenzene to hexamethylbenzene) were also rotated about the axis perpendicular to the center of the ring resulting in < 5 kJ mol^{-1} energy decreases for C_7H_8* at O14 and O16, but a ~45 kJ mol^{-1} decrease at O25 (Fig. 3c).

States with co-adsorbed species, such as C_6H_6--CH_3OCH_3* (Fig. 3b), may contain both acid-site interacting fragments (CH_3OCH_3*) and non-interacting fragments (C_6H_6). These two fragments were rotated independently of each other. Benzene was rotated with spatial reorientations (e.g., Fig. 2c) and CH_3OCH_3 was rotated with acid site reorientations (e.g., Fig. 2a). The reorientation that located the minimum value is the rotation about the c-axis angle at O14, a-axis at O16, and Al–O_a–A_1 at O25—suggesting that no single reorientation scheme consistently finds the minimum energy state. Internal reorientations are specific to ring methylation transition states (concerted or via methoxy species, Fig. 3e,f). Both ring methylation transition states, $[C_6H_6\cdots CH_3\cdots Z]^{\neq}$ (sequential) and $[CH_3OH\cdots CH_3\cdots CH_6H_6]^{\neq}$ (concerted), underwent internal reorientations (e.g. Fig. 2b) in addition to the other appropriate reorientations (acid site reorientations in sequential methylation and spatial reorientations in concerted methylation). The orientation of the ring was changed independently of the transition state (about the O_m–C_1–C_2 axis); these reorientations resulted in an average decrease of 12 kJ mol^{-1} for transition states relevant to benzene methylation. The internal coordinates of the CH_3OH and attacking methyl species were also altered about the O_m–C_1–C_2 axis resulting in energy decreases of 16 kJ mol^{-1} and 19 kJ mol^{-1}.

Initial optimizations or transition states formed by manually generated structures or pathways are consistently less stable than the best structures obtained by their systematic reorientation. These energy shifts can be as high as 45 kJ mol^{-1} and are not consistent across all adsorbates, indicating that the absence of these reorientation calculations significantly affects ground-state activation barriers and reaction energies. Performing these systematic reorientations leads to major shifts in DFT-predicted reaction mechanisms, kinetics, and surface coverages. No consistent reorientation schemes or types (e.g., acid site) locate the lowest energy state; therefore, when using static DFT reorientations to probe a potential energy surface, all appropriate reorientation schemes should be utilized to obtain the lowest energy state.

Surface methylation reactions were modeled on all four T11 O-sites (O14, O16, O24, and O25) with both CH_3OH and CH_3OCH_3 (Fig. 4). Observed free energy barrier trends for both methylation agents are identical with regards O-site preference (O16 < O14 < O25 < O24), suggesting methylation transition states on sites near the straight channel are more stable. Initial calculations (pre-reorientation) followed different trends for transition state stabilities on these O-sites (Fig. S6). These results further demonstrate the necessity of seeding the potential energy surface with systematically reoriented structures to find the lowest energy transition states. These data also suggest that reaction energies cannot predict the kinetically active site, as reaction energies do not trend with the stability of activation barriers.

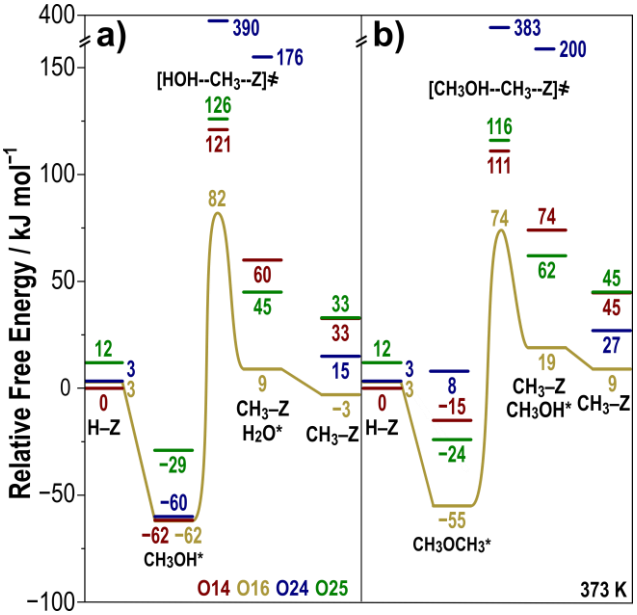

Figure 4. Reaction coordinate diagram of surface methylation by **a)** CH_3OH, and **b)** CH_3OCH_3 (right) at O14 (red), O16 (yellow), O24 (blue), and O25 (green). The most favorable pathway, determined by the lowest energy transition state, occurs at O16 and is traced with lines. Free energy values relative to a proton at O14 are reported at 373 K in kJ mol^{-1}.

The transition states on O14, O16, and O25 sit in the straight channel (Fig. 5), where stabilizing interactions between the framework and transition state complex are maximized. The transition state for surface methylation with CH_3OH at O16 forms the strongest H-bonds with the framework (182 pm, Fig. 5b), leading to the most stable transition state for surface methylation with CH_3OH. Similarly, the transition state from CH_3OCH_3 at O16 forms H-bonds with the framework (192 pm) which are shorter than those found in transition states at O14 and O25 (221 pm and 215 pm respectively, Fig. 5 a,d). Both transition states at O24 form H-bonds (192 pm for CH_3OH and 188 pm for CH_3OCH_3, Fig. 5c), but because O24 does not share a void with O14, O16 and O25, the transition state nearly collides with framework atoms. As a result, repulsive forces outweigh the stabilization conferred by H-bonding, leading to a barrier >200 kJ mol^{-1} higher than the barrier at all other O-sites.

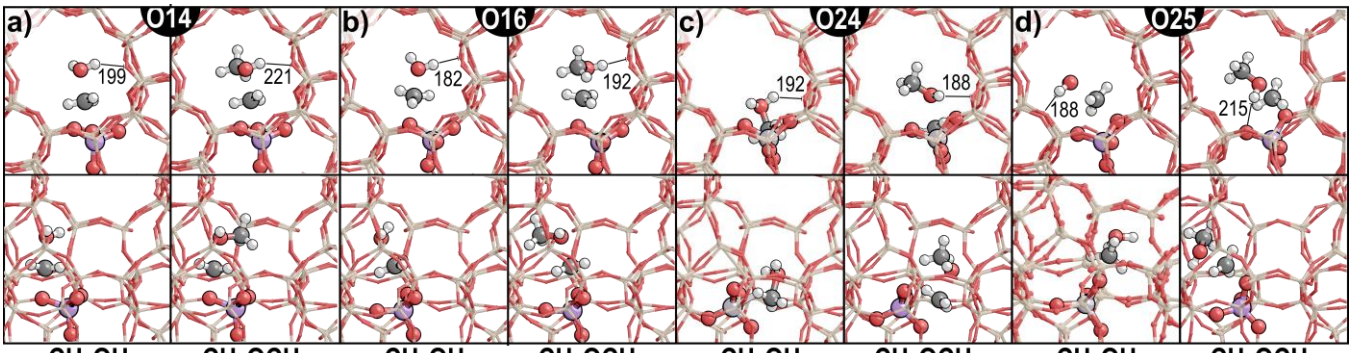

	CH_3OH	CH_3OCH_3	CH_3OH	CH_3OCH_3	CH_3OH	CH_3OCH_3	CH_3OH	CH_3OCH_3
ΔH	60	54	20	14	318	317	61	54
ΔS	−165	−161	−165	−161	−194	−190	−169	−165
ΔG	121	111	82	74	390	383	125	116

Figure 5. Lowest energy orientation of the surface methylation transition state at **a)** O14, **b)** O16, **c)** O24, and **d)** O25 looking down the straight (top) and sinusoidal (bottom) channels for CH_3OH and CH_3OCH_3. Enthalpy (kJ mol^{-1}), entropy (J mol^{-1} K^{-1}), and free energy (kJ mol^{-1}) values are reported at 373 K and relative to a protonated zeolite and stoichiometric amounts of gas-phase CH_3OH or CH_3OCH_3 molecules, as appropriate. Relevant H-

bond lengths are reported in pm. Additional viewing angles for the methylation of O24 are provided in Fig. S7 in the Supporting Information.

Examining these reactions at all O-site combinations and reorienting optimized reactant, product, and transition state structures results in activation free energies varying from 82 to 126 kJ mol^{-1} (neglecting the nearly inaccessible O24 site). Furthermore, systematic reorientations (e.g. Fig. 2) shift energies by ~10 kJ mol^{-1} on average and up to 45 kJ mol^{-1} compared to calculations optimized from 'manually' generated structures, typical of DFT examinations. These reorientations were done for all calculations in this text, although only discussed in this section. These efforts demonstrate the complexity of the potential energy surface for zeolite-catalyzed reactions, in contrast to metal surface reactions, for example, which have relatively few binding modes of interest for each adsorbate. While ab initio molecular dynamics have been used previously to determine low-energy states in MTH studies,[33] we feel these systematic reorientation studies offer a less computationally expensive approach for determining ground state energetics of adsorbates and transition states within zeolites for thermodynamic and kinetic analyses.

3.2 Kinetics of Benzene Methylation

Arene methylation can occur through two well-defined mechanisms[1,6,11]: sequential and concerted methylation. Rate equations for each possible rate-determining step are used to employ a maximum rate analysis which asserts, one at a time, that a step is rate-determining and that all preceding steps are quasi-equilibrated. This method of rate analysis can be used to predict the maximum net rate for each elementary step using DFT-calculated energies. Maximum rate analysis permits identification of the rate-determining step (that with the lowest maximum rate in a pathway) and allows for direct comparison of experimentally obtained rates to those obtained from DFT. All rates are determined from transition state theory with activation entropies contributing to pre-exponential factors. Rate equations are derived based on the assumption of a single adsorption site that may contain isolated species (such as CH_3OR^* or $C_xH_y^*$) or complexes in which two species are adsorbed concurrently (such as C_xH_y--CH_3OR^*, which represents CH_3OH or CH_3OCH_3 and an arene present in the pore). All adsorption steps are assumed to be quasi-equilibrated and are represented by equilibrium constants as defined in Fig. 6 and product desorption is assumed to occur instantaneously upon product (CH_3OH and H_2O) formation. These rate equations are defined and derived in Section S2 of the Supplemental Information.

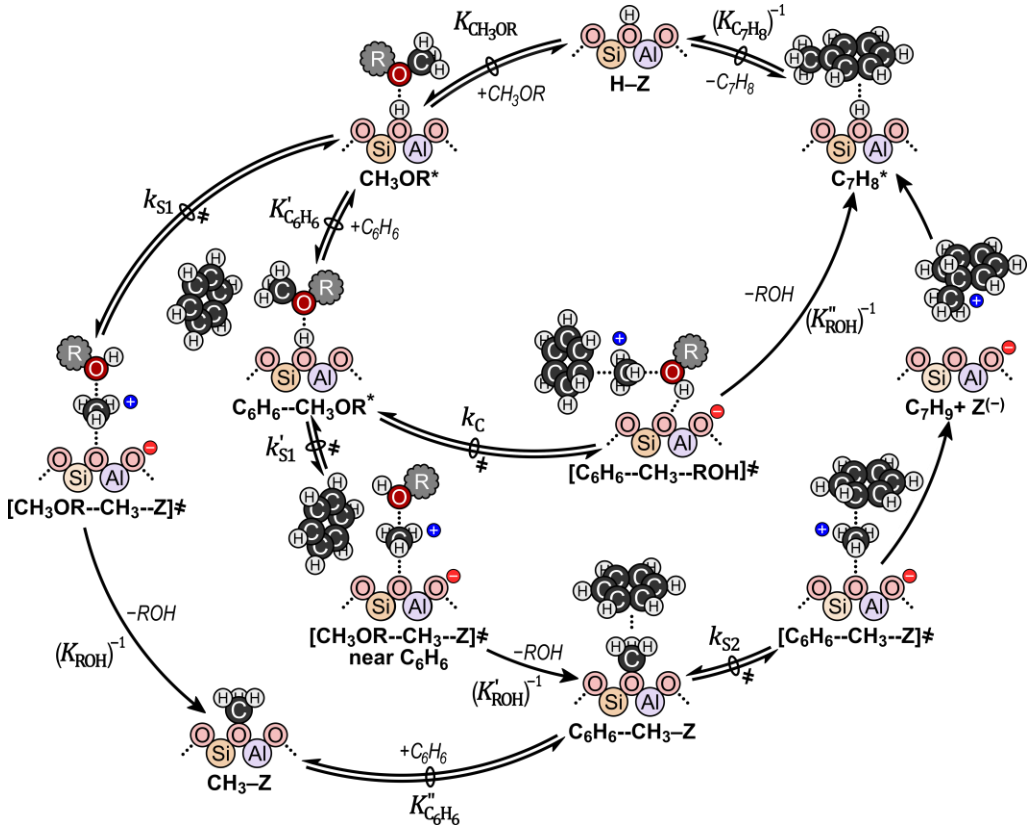

Figure 6. Scheme of benzene methylation pathways showing surface methylation with no spectating species, surface methylation with spectating benzene, concerted methylation, and deprotonation (left to right). Associated rate constants (K and k values) are shown adjacent to each arrow and are used in Eq. 4.

The preferential mechanism of benzene methylation is analyzed using DFT-obtained activation and reaction free energies to evaluate the rate equations derived in Section S2 through maximum rate analysis. The maximum rates of the concerted and sequential pathways are compared to determine the preferred mechanism. Maximum rate analyses can be used to compare reactions that occur in parallel, for example surface methylation in an empty pore versus surface methylation with a spectating arene, by identifying the mechanism with the highest possible rate which is most likely to form the product. Alternatively, the maximum rate of reactions that occur in series—for example surface methylation followed by ring methylation of the sequential mechanism—is determined by identifying the step with the lowest maximum rate which limits the rate of that pathway. Maximum rate analysis also allows for comparison of DFT-derived rates and experimentally measured rates. We compare our predictions to measurements obtained from kinetic studies of benzene methylation by CH_3OCH_3 (373 K, 0.02 bar aromatic, 0.68 bar CH_3OCH_3, 0.1% aromatic conversion).[28]

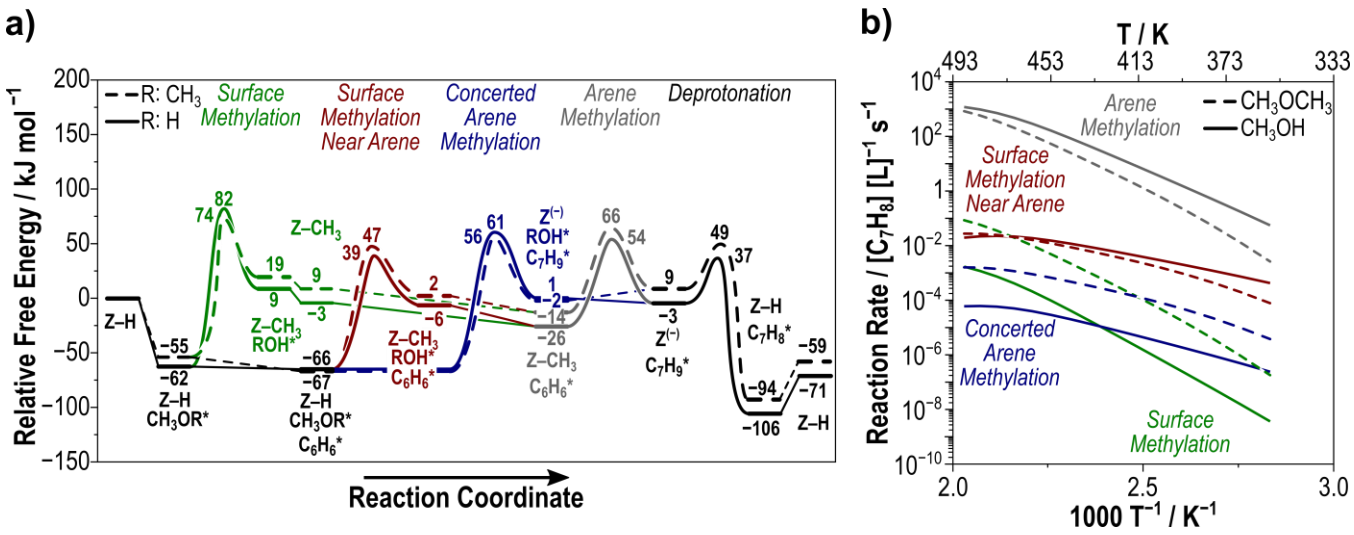

Figure 7. **a)** Reaction coordinate diagram with free energies (kJ mol^{-1}, 1 bar, 373 K) relative to a proton at O16 for benzene methylation by CH_3OH (solid lines) and CH_3OCH_3 (dashed lines) with surface methylation (green), surface methylation near arene (red), concerted arene methylation (blue), arene methylation (gray), and deprotonation (black) steps. **b)** Maximum rates of arene methylation by CH_3OH (solid) and CH_3OCH_3 (dashed) at 0.01 bar C_6H_6, 0.68 bar CH_3OR, 0.1% aromatic conversion, ranging from 353–493 K using surface methylation of O16 (green), surface methylation of O16 near arene (red), concerted arene methylation (blue), and arene methylation (gray) as the rate determining step.

Surface methoxy formation, the first step of the sequential mechanism, was investigated in an empty zeolite and with a spectating benzene ring with CH_3OH and CH_3OCH_3 at all four O-sites surrounding T11. Site O16, which is located in the channel intersection, has the lowest surface methoxy formation barrier with CH_3OH and CH_3OCH_3 (Section 3.1). At 353–463 K, the maximum rate of surface methylation with spectating benzene occurs with a higher maximum rate than surface methylation in an empty pore CH_3OH and CH_3OCH_3, demonstrating that benzene enthalpically stabilizes the surface methylation transition states (Fig. 7b). The rate increase with a spectating benzene is accompanied by concomitant decreases in the intrinsic free energy barriers at these temperatures: surface methylation by CH_3OH occurs with an intrinsic barrier of 144 kJ mol^{-1} in the absence of an arene co-adsorbate and 105 kJ mol^{-1} in the presence of one (Fig. 8) and a similar decrease from 129 kJ mol^{-1} to 114 kJ mol^{-1} is observed for CH_3OCH_3 at 373 K. Benzene provides enthalpic stabilization for surface methylation transition states at all temperatures; however, at higher temperatures, entropic gains from benzene desorption outweigh the enthalpic stabilization it confers. Surface methylation by CH_3OH has maximum rates that are slightly higher than CH_3OCH_3 when co-adsorbed benzene is present. These barrier differences, however, are within the uncertainty associated with DFT calculations (~10 kJ mol^{-1}). Therefore, it is reasonable to assume that both CH_3OH and CH_3OCH_3 are equally capable of methylating the MFI surface at site T11 in the presence of a co-adsorbed benzene.

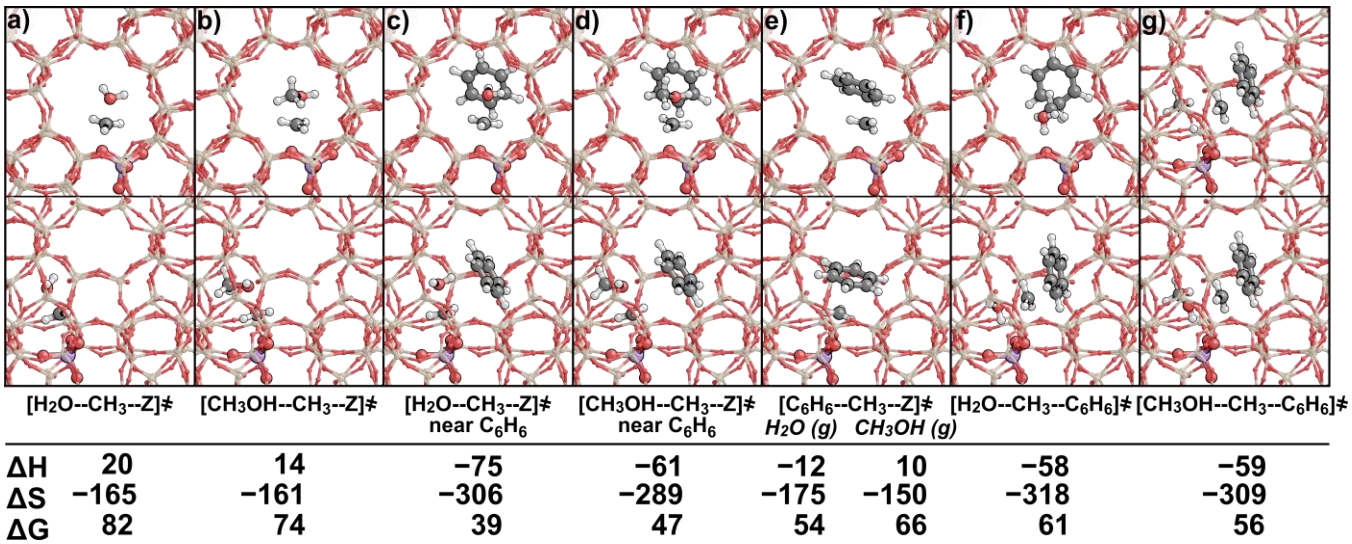

ΔH	20	14	−75	−61	−12	10	−58	−59
ΔS	−165	−161	−306	−289	−175	−150	−318	−309
ΔG	82	74	39	47	54	66	61	56

Figure 8. Lowest energy orientation of **a)** empty surface methylation with CH_3OH, **b)** empty surface methylation with CH_3OCH_3, **c)** surface methylation with spectating benzene with CH_3OH, **d)** surface methylation with spectating benzene with CH_3OCH_3, **e)** benzene methylation via surface methoxy, **f)** concerted methylation with CH_3OH and **g)** concerted methylation with CH_3OCH_3 with views down the straight (top) and sinusoidal (bottom) channels. Enthalpy (ΔH in kJ mol^{-1}), entropy (ΔS in J K^{-1} mol^{-1}), overall free energy barriers (ΔG in kJ mol^{-1}) are reported at 373 K and relative to a proton at O14. Intrinsic free energy barriers for each transition state (ΔG_{int} in kJ mol^{-1}) are also reported at 373 K.

Here, systematic reorientations (Section 3.1) provided valuable insight to the cooperativity between co-adsorbates and the different voids of MFI—aspects that were unapparent on initial structure input. The surface methylation transition states occur with the lowest barriers when positioned in the straight channel, rather than the channel intersection, because the tighter confinement by the framework offers more dispersive stabilization (Section 3.1). When benzene is co-adsorbed during surface methylation, the transition states (CH_3OH and CH_3OCH_3) remain in the straight channel while the benzene caps the intersection of the straight and sinusoidal pores (Fig. 8 b,c). This orientation of benzene creates a pocket that increases dispersive stabilization without preventing diffusion and transport as the benzene can shift to allow ROH egress. The MFI framework thus offers a unique environment for catalysis as small transition states can be confined in the straight channel, while larger species can reside in the channel intersection, thereby maximizing stabilization for small species and minimizing steric repulsions for large species. This cooperativity between the smaller channels and larger intersections makes MFI ideal for reactions involving disparately sized species such as those involved in benzene, toluene, and xylene (BTX) methylation and MTH reactions.

Benzene methylation via CH_3–Z is rapid compared to the formation of CH_3–Z species, occurring at rates over 100× higher at 373 K. Ring species are methylated most favorably from surface methoxies bound to O16, which is also the most favorable O-site to form surface methoxy species. Systematic reorientations suggest that the lowest barrier transition state occurs when the benzene ring is oriented so that it is co-planar with the attacking methyl group (Fig. 8e). The transition state for arene methylation from a surface methoxy is the same for CH_3OH and CH_3OCH_3 methylating agents; however, different ROH leaving groups for the two methylating agents yield different maximum rates. Differences in the formation and desorption energies of these ROH species—resulting from entropic contributions of the leaving group upon desorption—cause the maximum rate of arene methylation to be higher than that of surface methylation at temperatures >353 K (temperatures relevant to arene methylation and MTH). This indicates that the rate of sequential methylation is limited by the rate of forming surface methoxy

species and that the maximum rate of the consumption of CH_3–Z is rapid relative to their formation at 0.1% conversion.

The pressure of the ROH leaving group, and thus the conversion, can alter the rate-determining step of the sequential mechanism. Arene methylation reactions are typically run at low arene conversions (0.1% here) and thus the pressure of ROH leaving group (0.00002 bar) is very low relative to the pressure of CH_3OR (0.68 bar). Rates of surface methylation are not dictated by ROH pressures at negligible conversions, where equilibrium effects need not be considered. Rates of arene methylation from surface methoxy groups, however, are inhibited by ROH pressures and thus dependent on conversion, X

$$r = k_{S2} K_{CH_3OR} K'_{S1} K'_{C_6H_6} P_{C_xH_y,0} \frac{(1-X)\left(\frac{P_{C_xH_y,0}}{P_{CH_3OR,0}} - X\right)}{X} \quad (4)$$

Increasing the conversion from 0.1% to 0.2% would cause a ~2× decrease in the rate of ring methylation via the concerted mechanism whereas the same conversion increase would negligibly impact rates if the concerted mechanism or surface methylation were the rate-determining steps (rate constants for Eq. 4 is defined in Fig. 6 and derived in Section S2). As the pressure of the ROH group increases with increasing conversion, the formation and subsequent desorption of the ROH leaving group results in an inhibition of the benzene methylation through the action of Le Chatelier's principle. The rate of surface methoxy formation will approach equilibrium, thus limiting consumption of surface methoxy species by benzene and decreasing the rate of arene methylation (Fig. 9, gray). This kinetic behavior is also observed, for example, in the hydrogenolysis of alkanes on metal surfaces, in which H_2(g) is formed in quasi-equilibrated dehydrogenation steps prior to the rate-determining C–C bond activation.[60–62] At benzene conversions above ~20% for CH_3OH and CH_3OCH_3, the rate of CH_3–Z consumption by benzene becomes limited to the extent that benzene methylation becomes rate determining in the sequential pathway (Fig. 9). At very high benzene conversions (> 75%) for CH_3OCH_3, the concerted pathway occurs with nearly identical rates to the sequential pathway. These strong effects of ROH pressure at low conversion are only observed if arene methylation is the rate determining step (i.e., the rate is dependent on the pressure of ROH) lending importance to those experimental studies for this and similar methylation reactions (e.g., alcohol dehydration).[1] This inhibition via Le Chatlier's principle, unlike site-blocking inhibition, is observable across all pressure ranges of the ROH leaving group indicating that is can be observed or ruled out by simple space velocity experiments, rarely published but often performed.

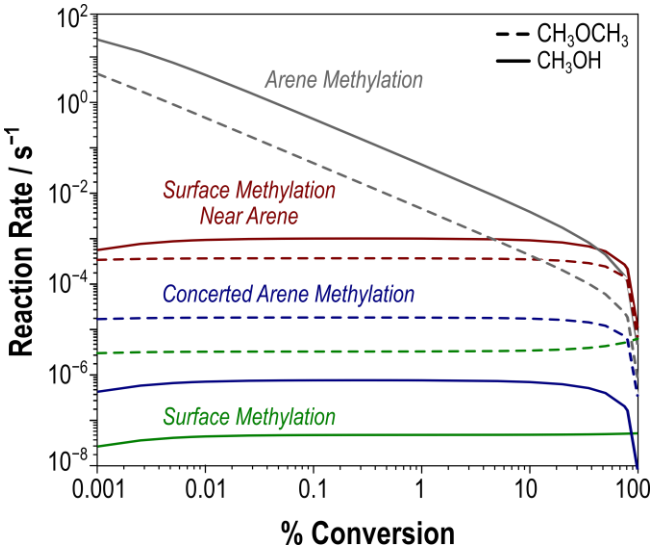

Figure 9. Rate of arene methylation (gray), surface methylation near arene (red), concerted methylation (blue), and surface methylation in an empty pore (green) with CH_3OH (solid lines) and CH_3OCH_3 (dashed lines) from 0.1–100% CH_3OR conversion at 0.68 bar CH_3OR, 0.02 bar C_6H_6, 373 K.

The concerted and rate-determining step of the sequential mechanism, surface methylation with spectating benzene, demonstrate the same pressure dependencies in the rate equation (Eqs. S7 and S19) making it difficult to use kinetic experiments to differentiate the two mechanisms, motivating this DFT study. Similarly, the presence or absence of CH_3–Z species does not necessarily support that the sequential mechanism occurs or preclude the concerted mechanism from occurring. The most favorable orientation of the transition state associated with concerted benzene methylation involves a hydrogen bond between deprotonated O16 and the leaving group species (H_2O or CH_3OH, Fig. 8f,g). Concerted methylation of benzene by CH_3OCH_3 (58 kJ mol^{-1}) is slightly more favorable than methylation by CH_3OH (62 kJ mol^{-1}); however, these values fall within the uncertainty of DFT, indicating that the relative rates of methylation by these two species should be nearly proportional to their pressure ratios. Overall free energy barriers of concerted methylation can be directly compared to those of the rate-determining surface methylation step as the two reactions demonstrate the same pressure dependencies. Barriers of concerted methylation are 20 kJ mol^{-1} higher for CH_3OH and 30 kJ mol^{-1} higher for CH_3OCH_3 than the barriers of surface methylation (Fig. 7a), indicating that sequential methylation is the preferred mechanism at these conditions and 0.1% conversion. However, at conversions above 75% for CH_3OCH_3 the maximum rate of the sequential mechanism (determined by the maximum rate of arene methylation, Fig. 9) is limited and the concerted mechanism becomes preferred as arene methylation rates from CH_3–Z slow.

Only direct proton donation from $C_7H_9^+$ to the zeolite surface was modeled to approximated deprotonation barriers. In a real system, CH_3OH or H_2O can act as proton shuttles and facilitate proton transfer to the zeolite surface and the barriers in the presence of these species could be lower. The rate of deprotonation, however, is significantly higher than the rate of other possible rate determining steps for benzene methylation (Fig. S8). Deprotonation benefits from relatively low barriers (Fig. 7) coupled with entropic contributions of oxygenate desorption. As such, it does not limit methylation rates and will not be discussed in the remainder of this work because of its kinetic irrelevance.

Surface MASI were calculated using a Langmurian adsorption model, using DFT-obtained adsorption energies to identify abundant surface intermediates. Possible MASI are limited to CH_3OR*, C_6H_6*, CH_3–Z, C_6H_6--CH_3OR*, and C_6H_6--CH_3–Z in this analysis. CH_3OH* is the predominant MASI from 353–473 K when CH_3OH serves as the methylation agent. At temperatures above 473 K, the MASI becomes CH_3–Z, suggesting that surface methylation occurs in an empty pore at these temperatures, likely because adsorption of C_6H_6 is limited as the temperature increases (Fig. S10). When CH_3OCH_3 serves as the methylation agent, C_6H_6--CH_3OCH_3 is the MASI between 353–373 K, suggesting that adsorption of C_6H_6 is facile at low temperatures. Between 383 and 493 K, the MASI becomes predominantly CH_3OCH_3, because C_6H_6 adsorption is less favorable at high temperatures. At temperatures above 473 K, CH_3–Z species begin to appear on the surface (20–40%); however, the formation of CH_3–Z is kinetically limited at low temperatures. Maximum rate analyses do not predict that CH_3–Z species are the MASI between 353 and 493 K—only at temperatures above 503K are CH_3–Z species observed to cover the surface (Fig. S9).

Previous experimental studies of C_6H_6--CH_3OCH_3 reactions used kinetic data isotopic labeling studies, and post-reaction titration studies to conclude that benzene methylates via the sequential pathway and that the arene alkylation step is rate determining on sites covered by CH_3–Z species.[28] These kinetic studies showed a linear dependence on benzene pressure (Fig. 10), indicating that benzene adsorption occurs prior to the rate determining step, suggesting arene methylation is the rate determining step. However, we have shown that surface methylation

also occurs after benzene adsorption as it is facilitated by co-adsorbate interactions, which yields similar kinetic behavior (Eqs. S7 and S19). The zero-order dependence in CH_3OCH_3 pressure indicates that the MASI is derived from CH_3OCH_3, such as CH_3OCH_3*, CH_3–Z, or C_6H_6--CH_3OCH_3* (co-adsorbed). Our DFT calculations, however, suggest that CH_3–Z is never a MASI at these conditions as it quickly consumed by co-adsorbed C_6H_6 and surface methylation never approaches equilibrium because of the low CH_3OH content (0.0002 bar). Isotopic studies demonstrate that when feeding d_0 and d_6 CH_3OCH_3 at benzene methylation conditions, there is 1:2:1 d_0:d_3:d_6, suggesting facile C–O cleavage, and our calculated barriers concur. However, the low CH_3OH content prevents scrambling via reversible surface methylation reactions and this scrambling is more likely explained by the formation and decomposition of trimethyloxonium species:

$$CH_3OCH_3 + CH_3\text{–}Z \rightarrow [(CH_3)_2O\cdots CH_3^+\cdots Z^-]^{\ddagger} \rightarrow (CH_3)_3O^+ + Z^- \quad (5)$$

which occurs with low barriers (60 kJ mol^{-1}). This indicates rapid exchange of CH_3 between CH_3OCH_3 and the zeolite surface, resulting in the observed d_0:d_3:d_6 ratios, as shown in Section S3. Post-reaction titration studies (H-SPP heated to 423 K to remove physisorbed species) with flowing H_2O form CH_3OH in a 1:1 ratio with Al content, indicating that the heated material was covered with CH_3OH* or CH_3–Z, the former being more likely.[28] The concentration of CH_3–Z, however, is very sensitive to the pressure of C_6H_6, CH_3OH, and H_2O in the system. The heat treatment to remove physisorbed species could have created a surface covered in CH_3–Z; these purge tratements are typical of zeolite methylation protocols for this reason. Instead, our DFT calculations suggest that a mixture of CH_3OCH_3* and co-adsorbed C_6H_6--CH_3OCH_3* dominate the surface at benzene methylation conditions; this is consistent with the observed zero-order pressure dependence in CH_3OCH_3. However, this analysis predicts a sub-linear kinetic behavior in C_6H_6 (rather than the linear behavior observed). This disagreement with experimental evidence is caused by the C_6H_6 binding free energy calculated here (–11 kJ mol^{-1}), which is approximately 4 kJ mol^{-1} more exothermic than that found from experiments.[28] Increasing the binding energy to –7 kJ mol^{-1} ad hoc results in a linear dependence on benzene pressure, consistent with measured kinetic data.[28] This thermodynamic correction does not cause CH_3–Z to become a predicted MASI, however, because with these altered data CH_3OCH_3* are predicted as the lone MASI at the conditions of the prior kinetic study.

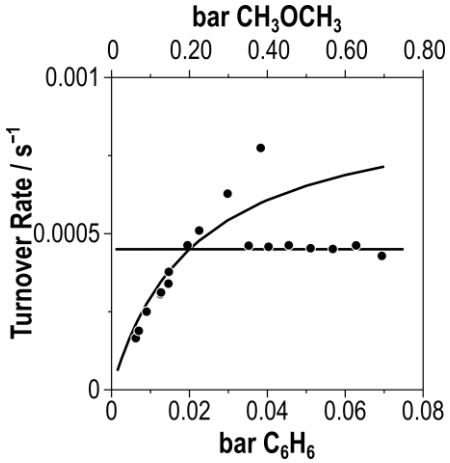

Figure 10. Comparison of DFT-obtained turnover rates with CH_3OCH_3 (solid) and experimentally obtained rates (circles) multiplied by a factor of 17 from Ref. 28. Data points are reported at 373 K, 0.2 bar C_6H_6, 0.68 bar CH_3OCH_3, and 0.1% aromatic conversion.

3.3 Mechanisms of Toluene Methylation

Toluene methylation yields three unique products: *ortho*-, *meta*-, and *para*-xylene. *Para*-xylene has the highest industrial relevance as it is a precursor to terephthalic acid.[63] Xylene selectivity typically favors the formation of *meta*-xylene;[64] however, zeolites, particularly H-ZSM-5, can shift this selectivity to favor para-xylene production through diffusive restrictions.[65–68] Here, the mechanisms and rates of toluene methylation are analyzed using the previously discussed maximum rate analysis method (Fig. 11) to determine the intrinsic selectivities of the active site, uncorrupted by mass transport limitations. These insights can determine whether the observed preference for para-xylene is caused solely by mass transport limitations or if those limitations bolster a kinetically favored pathway.

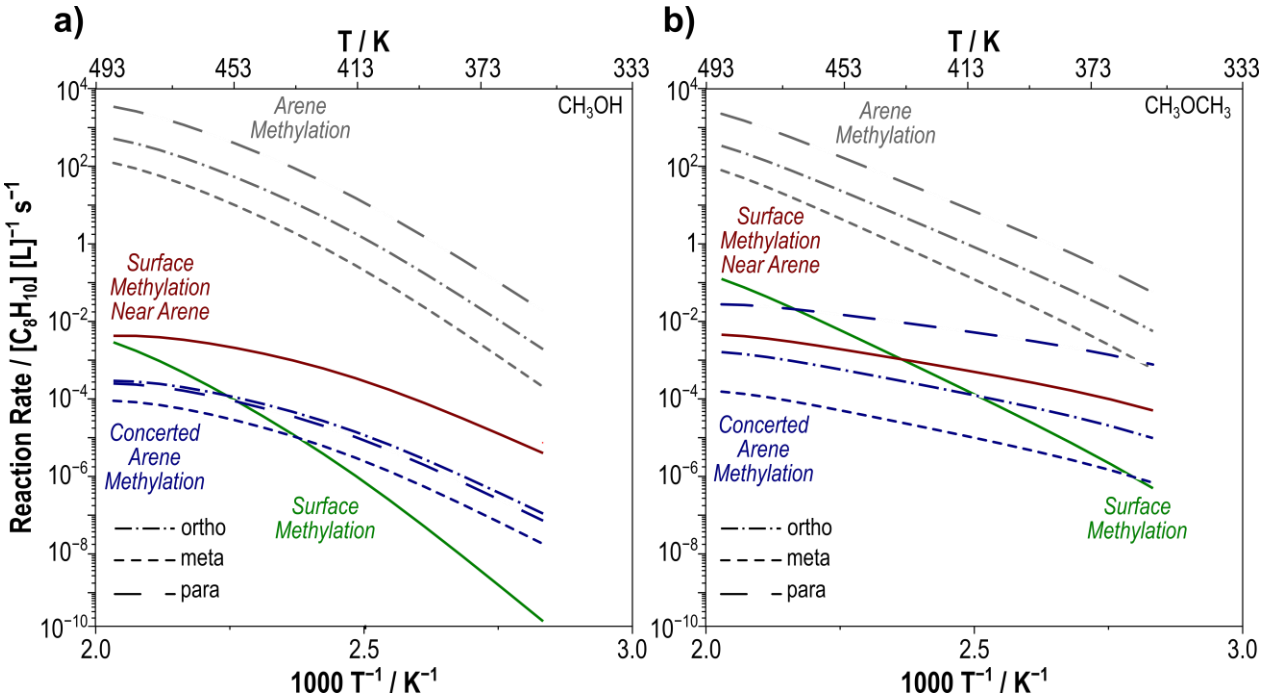

Figure 11. Maximum rates of sequential ring methylation (gray), surface methylation of O16 with benzene (red), surface methylation in an empty pore (green), and concerted methylation (blue) for *ortho*-, *meta*-, and *para*-xylene formation with **a)** CH_3OH and **b)** CH_3OCH_3 at 0.03 bar C_7H_8, 0.68 bar CH_3OR, 0.1% aromatic conversion, ranging from 353 K to 493 K.

Surface methylation in the presence of toluene demonstrates the same pore cooperativity as benzene (Section 3.2) to maximize non-covalent interactions and thus lower transition state barriers as compared to surface methylation in an empty pore. Surface methylation in the presence and absence of toluene occurs most favorably on O16. Both the CH_3OH and CH_3OCH_3 transition states reside in the straight channel to maximize dispersive interactions. Toluene resides in the channel intersection and acts as a channel 'cap' to maximize dispersive interactions (shown in Fig. 12) and the surface methylation transition state resides in the straight channel to maximize favorable non-covalent interactions with the framework (such as H-bonding, c.f., Fig. 5). The presence of toluene lowers intrinsic barriers associated with CH_3OH surface methylation from 144 to 125 kJ mol^{-1}; similarly, the barrier for methylation by CH_3OCH_3 decreases from 130 kJ mol^{-1} to 114 kJ mol^{-1} at 403 K and 1 bar of all species. At toluene methylation conditions (403 K, 0.05 bar C_7H_8, 0.68 bar CH_3OR, 0.1% aromatic conversion), surface methylation with spectating toluene occurs at a higher maximum rate than surface methylation in an empty pore. This suggests that CH_3–Z is primarily formed with spectating toluene at these conditions. However, at temperatures above 503 K for CH_3OH and 423 K for CH_3OCH_3, the rate of surface methylation in an empty pore occurs at a higher maximum rate than with spectating toluene. This likely occurs

because the strongly exothermic nature of toluene adsorption (ΔH_{ads} of −94 kJ mol^{-1}) becomes less favorable as the temperature increases. Surface methylation by CH_3OCH_3 occurs with rates only 1.5× faster than those with CH_3OH at 403 K, suggesting that CH_3OCH_3 and CH_3OH are equally capable of methylating the surface (Fig. 11).

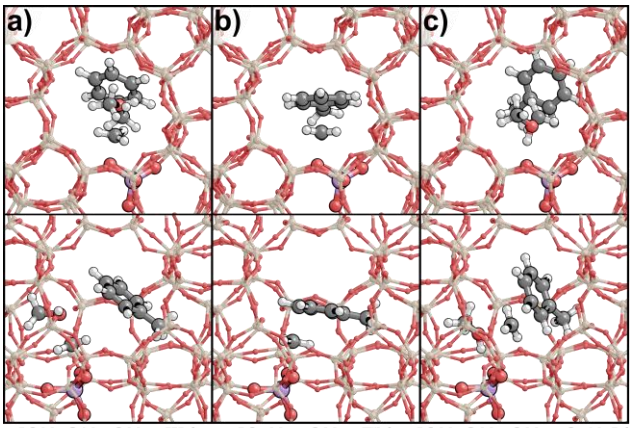

Figure 12. Lowest energy orientation for **a)** surface methylation, **b)** ring methylation (*para*-xylene formation shown), and **c)** concerted methylation (*para*-xylene formation shown) with CH_3OCH_3 with views down the straight (top) and sinusoidal (bottom) channels. Enthalpy (kJ mol^{-1}), entropy (J K^{-1} mol^{-1}) and free energy (kJ mol^{-1}) are reported at 403 K and relative to a proton on O14.

The rate of ring methylation via the sequential mechanism, like benzene methylation, occurs most favorably at O16 and has maximum rates > 200× higher than those for surface methylation at toluene methylation conditions (Fig. 11b), indicating that the rate of ring methylation is limited by the formation of surface methoxy species. Therefore, surface methylation with spectating toluene is the rate-determining step of the sequential mechanism of toluene methylation with CH_3OH and CH_3OCH_3. Although ring methylation does not control the rate of sequential methylation, it does control the selectivity towards *ortho*-, *meta*-, or *para*-xylene. Ring methylation selectivity favors *para*-xylene, then *ortho*-xylene, and finally *meta*-xylene (Fig. 11), suggesting that para-xylene is the kinetically preferred product of the sequential mechanism; this neglects additional effects of mass transport that would prevent egress of *ortho*- and *meta*-xylene in practical studies. Such high para-xylene selectivity is not observed in experimental studies (573 K, 0.015 bar CH_3OH, 0.06 bar C_7H_8, and 4.3% C_7H_8 conversion) which have demonstrated that xylene distribution only slightly favors para-xylene formation, with distributions of 35% *ortho*-, 28% *meta*-, and 38% *para*-xylene.[69] At the same conditions, DFT results suggest the distribution is 13% *ortho*-, 4% *meta*-, and 83% *para*-xylene; however, these distributions arise from arene methylation barriers that differ by only 12 kJ mol^{-1} (Fig. 13), near the expected error in DFT calculations. Despite the uncertainties in these DFT-predicted selectivities, the trends suggested by DFT follow those found in experiment, where *para*-xylene is preferred over *ortho*-xylene and *meta*-xylene. While DFT cannot accurately predict selectivities of products of these reactions, it can predict trends based on estimated free energy barriers and thus elucidate experimental results convoluted by mass transport limitations.

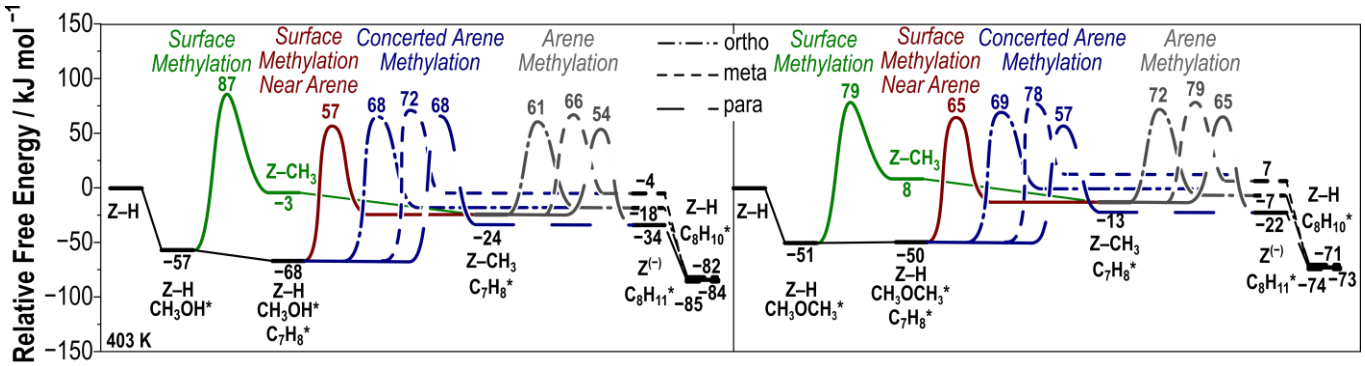

Figure 13. Reaction coordinate diagram of toluene methylation to form *ortho*-, *meta*-, and *para*-xylene with CH_3OH (left) and CH_3OCH_3 (right) via the sequential (at O16) and concerted mechanisms. Free energy barriers are reported at 403 K, 1 bar.

The concerted methylation of toluene has three possible transition states (forming each xylene) for each methylation agent, all of which strongly H-bond with deprotonated O16 to stabilize the ROH leaving group. Here, free energy barriers of concerted methylation can be directly compared to those of surface methylation with spectating toluene to determine the preferential toluene methylation route as both mechanisms demonstrate the same pressure dependencies. When CH_3OH serves as the methylation agent, surface methylation occurs with a lower barrier (57 kJ mol^{-1}) as compared to concerted methylation to form *ortho*- (68 kJ mol^{-1}), *meta*- (73 kJ mol^{-1}), and *para*-xylene (73 kJ mol^{-1}). The sequential mechanism occurs with barriers over 10 kJ mol^{-1} lower than those of the concerted mechanism when CH_3OH serves as the methylation agent, suggesting that sequential methylation is the predominant mechanism through which CH_3OH methylates toluene. When CH_3OCH_3 is the methylation agent, the barrier to methylate the surface (65 kJ mol^{-1}) is less than concerted barriers to form *ortho*- (69 kJ mol^{-1}) and *meta*-xylene (79 kJ mol^{-1}), but higher than the concerted barrier to form *para*-xylene (57 kJ mol^{-1}, Fig. 13). Therefore, when CH_3OCH_3 is the methylation agent, *para*-xylene is formed via the concerted mechanism preferentially over CH_3–Z species and other xylene isomers. Barriers to form *para*-xylene are 7–21 kJ mol^{-1} lower than those to form *ortho*- or *meta*-xylene, indicating that the intrinsic selectivity favors the formation of *para*-xylene and its formation is likely further promoted by mass transport restrictions disfavoring the desorption of *ortho*- and *meta*-xylene from the catalyst compared to the more-linear para isomer.

Para-xylene is the most favorable product to form for both CH_3OH and CH_3OCH_3; however, methylation to form *para*-xylene occurs through different mechanisms with CH_3OH (sequential methylation) and CH_3OCH_3 (concerted methylation), suggesting that the preferred methylation mechanism is dependent on both position of methyl-addition and methylation agent. Neither CH_3OH nor CH_3OCH_3 has proven a noticeably superior methylating agent among all methylation locations examined thus far (benzene and toluene); DFT-predicted barriers for each species differ by < 20 kJ mol^{-1} (Fig. S10).

Similar to Section 3.2, surface MASI were calculated using a Langmurian adsorption model with the same potential MASI, except with toluene instead of benzene (prediction of surface MASI are shown in Fig. S11) and are demonstrated to be both temperature and methylation agent dependent. When CH_3OH is the methylation agent, C_7H_8--CH_3OH* is the MASI at temperatures below 413 K; however, as the temperature increases C_7H_8 adsorption becomes less favorable and the MASI becomes a mixture of C_7H_8--CH_3OH* and CH_3OH* at temperatures above 413 K. As with benzene, entropic effects for larger arene species limit adsorption at higher temperatures, where high-entropy gas-phase species are favored. When CH_3OCH_3 is the methylation agent, CH_3OCH_3* is the MASI all temperatures (353–493 K), because toluene does not bond as strongly next to CH_3OCH_3 (ΔG_{ads} = −50 kJ mol^{-1}) as it does near CH_3OH (ΔG_{ads} = −68 kJ mol^{-1}) (Fig. 13).

The DFT results of toluene methylation suggest that toluene methylation via CH_3OCH_3 likely occurs via concerted mechanism with barriers ~8 kJ mol^{-1} lower than those of surface methylation. This value falls within the uncertainty of DFT, so it is difficult to determine which, if any, mechanism prevails at these conditions. Similar to benzene methylation, DFT-predictions can be used to provide insight and alternative explanations for previously published kinetic, surface titration, and isotopic switching results during CH_3OCH_3 and toluene co-reaction conditions (403 K, 0.008–0.08 bar C_7H_8, 0.68 bar CH_3OCH_3, 0.1% conversion).[28] Experimental kinetic results predict no dependence on CH_3OCH_3 pressure and a linear dependence on toluene pressure, from which the previous study concluded that the rate-determining surface methylation step occurred prior to toluene methylation. However, as we have shown with benzene and toluene methylation, surface methylation can occur in the presence of a spectating arene species, which explains the linear rate dependence on arene pressure. Furthermore, an abundance of CH_3OCH_3* on the surface explains a zero-order dependence on CH_3OCH_3 pressure. DFT results predict a linear dependence on toluene pressure and no dependence on CH_3OCH_3 pressure (Fig. 14), confirming that this species is the MASI, consistent with these previous kinetic studies. Isotopic switching studies also demonstrated a 1:2:1 mixture of d_0:d_3:d_6 when d_0 and d_6 CH_3OCH_3 were co-fed during toluene methylation.[28] Similar to benzene methylation, we suggest that this rapid exchange is likely to occur via trimethyloxonium species, not because surface methylation is a quasi-equilibrated step.

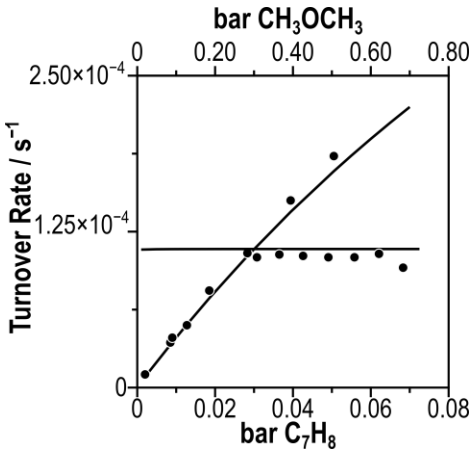

Figure 14. Comparison of DFT-obtained turnover rates with CH_3OCH_3 (solid) and experimentally obtained rates (circles) multiplied by a factor of 4 from Ref. 28. Data points are reported at 403 K, 0.03 bar C_7H_8, 0.68 bar CH_3OCH_3, and 0.1% aromatic conversion.

3.4 Mechanisms of Methylbenzene Methylation at Methanol-to-Hydrocarbon Conditions

Methanol-to-hydrocarbon (MTH) reactions typically occur at transient conditions because catalyst induction and deactivation preclude steady state operation. Industrially, this is overcome by operating in fluidized bed reactors with low catalyst residence times. MTH reacts at higher temperatures (523–723 K) than arene methylation conditions (373–473 K, 0.1% conversion), and can form a range of substituted methylbenzene co-catalysts which produce light alkenes in the aromatic cycle.[5,70,71] Here, we will analyze and interpret our arene methylation reactions at MTH conditions assuming 623 K, 0.04 bar C_xH_y, 0.08 bar CH_3OR, and 10 % conversion, similar to previous studies of MTH.[70]

Surface methylation was the rate-determining step of the sequential mechanism at low-temperatures (373–473 K) and low conversions (< 1%) and occurred near a spectating arene at benzene and toluene methylation conditions (373 K and 403 K, respectively). However, this trend is not observed in the rates of surface methylation at higher temperatures and near larger arene species (C_{9+}). Surface methylation in an empty pore is the preferred

mechanism for all species at MTH temperatures (near 623 K,) because arenes are less likely to co-adsorb at higher temperatures and larger arenes adsorb more weakly because of steric hindrance (Fig. S12). Larger arenes, however, do not adsorb into zeolite voids during MTH, instead, they are formed within those intersections and their limited diffusivities render them effectively trapped as co-catalysts. As C_6–C_{12} arenes will display a wide variety of diffusivities and adsorption energies, for the purposes of this section of the study, we consider all reactions taking place with or in the presence of a co-adsorbed arene. For example, to methylate a C_{10} arene, we assume that CH_3OCH_3 must either react with the arene in a concerted manner or methylate the surface in its presence because the arene species cannot desorb.

The maximum rates of ring methylation are over 1000× greater than the maximum rates of surface methylation (near a co-adsorbed arene) at MTH conditions for both CH_3OH and CH_3OCH_3 (Fig. S13). Therefore, the rate of surface methylation is the rate determining step for the sequential arene methylation pathway.

DFT-predicted rates of concerted methylation and sequential methylation pathways show no clear trends regarding the mechanism and the favorability of mechanisms can switch based on the choice of methylation agent. For instance, when methylating 1,2,4-trimethylbenzene to 1,2,3,5-trimethylbenzene with CH_3OH, the rate of concerted methylation is ~100× that of the sequential rate (correlating to a barrier difference of 18 kJ mol^{-1}, Fig. S14); however, the same reaction with CH_3OCH_3 occurs with sequential rates ~70× those of concerted methylation (corresponding to a barrier difference of 6 kJ mol^{-1}, Fig. S14). Concerted methylation rates tend to be within 50× of each other for CH_3OH and CH_3OCH_3 (Fig. S14), indicating that both species are viable methylating agents at MTH conditions. In general, the identity of the reactants dictates the preferred mechanism; for instance, all products of o-xylene methylation (Fig. 1 shows the products) are formed via the concerted mechanism with CH_3OCH_3 at MTH conditions while all products of m-xylene are preferentially formed via the sequential mechanism at the same conditions; this trend of reactants preferring the same methylation mechanism holds true for all methylbenzene species investigated. Overall, it is difficult to use trends to predict the predominant mechanism and methylation agent of arene methylation and it is likely that both mechanisms occur depending on the choice of methylation agent and number of spectating methyl-substituents.

The formation of higher methylbenzenes from benzene is of fundamental interest to determine active methylbenzene species during MTH reactions. Fig. 15 shows the lowest methylation barriers and the most facile chemical pathways to reach hexamethylbenzene. The formation of hexamethylbenzene from benzene proceeds through para-xylene, 1,2,4-trimethylbenzene, and 1,2,3,5-tetramethylbenzene—all of which have been identified as possible intermediates of the aromatic cycle in MTH chemistry by previous DFT and kinetic studies.[72–74] Fig. 15 shows these pathways for methylation via CH_3OH and CH_3OCH_3; both species prefer to proceed through the same intermediates to form hexamethylbenzenes, though some methylations occur via different pathways (sequential or concerted). Intrinsic methylation barriers vary from 76–137 kJ mol^{-1} but show no systematic trends with the number of methyl-substituents on the ring; therefore, forming C_{10+} species is likely feasible during MTH processes. This result contradicts previous theoretical studies which have predicted that methylation barriers decrease with additional methyl-substituents on the ring;[38] however, these studies were performed on zeolite cluster models and only investigated four ring interconversion pathways via the concerted mechanism—an insufficient analysis for these complicated pathways. The formation of higher methylbenzene species is thermodynamically favorable, with average reaction free energies of –34 kJ mol^{-1}. These reaction free energies increase with additional methyl substitution. For example, the formation of pentamethylbenzene from 1,2,3,5-tetramethylbenzene has a positive reaction free energy (+21 and +27 kJ mol^{-1} for CH_3OH and CH_3OCH_3, respectively). This indicates that extensively substituted rings start to encounter steric hindrance within MFI intersections, consistent with their less favorable adsorption energies (Table S2). Despite this, methylation

reactions are generally thermodynamically favorable and occur with barriers significantly lower than those reported for arene isomerization and alkene formation. This indicates that arenes either escape zeolite domains as aromatic products of MTH or become extensively substituted as C_{10}–C_{12} species that are trapped within MFI intersections. These highly substituted arenes can only serve as co-catalysts in the aromatic cycle[18,20,70,71] and ultimately grow to polyaromatic species[75–77] in deactivation mechanisms when trapped in zeolite pores.

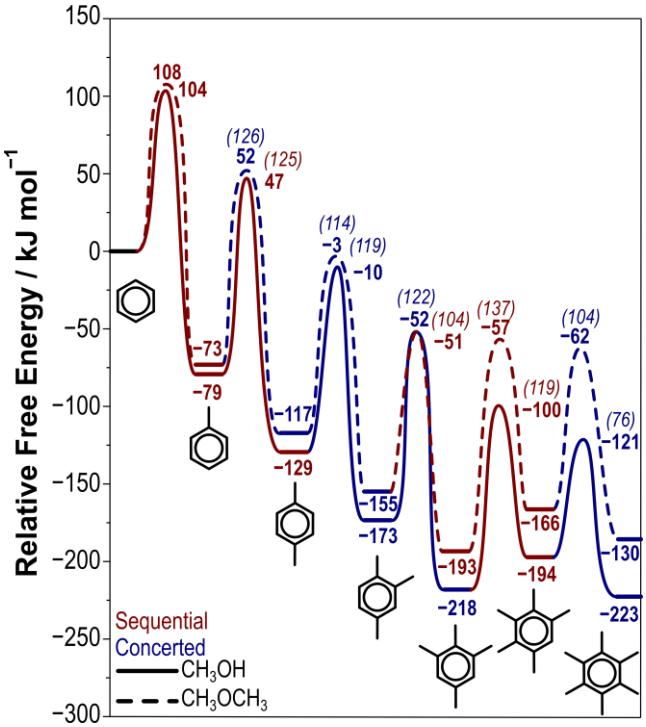

Figure 15. Reaction coordinate diagram of hexamethylbenzene formation via repeated benzene methylation with CH_3OH (solid lines) and CH_3OCH_3 (dashed lines). Overall barriers (relative to C_6H_6*) are shown in bold and intrinsic barriers are listed in italics and parentheses. Red lines indicate that the sequential mechanism is preferred, while blue lines indicate that the concerted mechanism is preferred. Barriers are reported at 623 K, 1 bar of all species.

4. Conclusions

Reactant, product, and transition state species involved in arene methylation reactions were systematically reoriented to probe the potential energy surface and identify their respective global minima. These reorientations demonstrate that a single optimization of a user-generated structure is insufficient to obtain reliable ground state energies. Reorientations reduced energies by up to 50 kJ mol^{-1} for states tested here. Furthermore, these systematic reorientations provide valuable insight regarding the void and co-adsorbate cooperativity, which are not immediately apparent. Through systematic reorientations of surface methylation transition states with co-adsorbed arenes, we have demonstrated that MFI offers a unique environment for catalysis because small transition states (e.g., surface methylation) can reside in the straight channel to maximize dispersive interactions while larger arenes (e.g., benzene) can reside in the channel intersection to minimize repulsive interactions with the zeolite framework. The proximity and locations of these species creates a ‘capped’ channel which resembles a side-pocket in which surface methylation is accelerated by non-covalent interactions among co-adsorbates and by solvation by the zeolite framework. This cooperativity of pores makes MFI an ideal catalyst for housing transition states of different sizes, such as those in BTX methylation and MTH reactions.

Concerted and sequential arene methylations were studied with CH_3OH and CH_3OCH_3 for all methylbenzene interconversion pathways from benzene to hexamethylbenzene. Maximum rate analyses were used to determine the rate determining steps of the sequential mechanism, compare the sequential and concerted mechanism, and compare DFT-predicted rates to previous kinetic studies. Benzene methylation is predicted to occur via sequential methylation at reasonable temperatures (353–623 K) and pressures (0.02–1 bar). Surface methylation facilitated by co-adsorbed benzene is rate-determining at these conditions with low benzene conversion (0.1%). However, at higher ROH pressures (caused by higher conversions, above 20%), the rate of surface methylation approaches equilibrium thus limiting the rate of the subsequent arene methylation reaction and causing it to become rate-determining. DFT data demonstrate that co-adsorbed benzene facilitates surface methylation by CH_3OH and CH_3OCH_3, resulting in rates that yield pressure dependencies identical to those observed experimentally. Additionally, isotopically labeled methyl groups in CH_3OCH_3 can be scrambled through trimethyloxonium cations, and surface methoxy species are only MASI in the absence of CH_3OH, H_2O, and C_6H_6 (i.e., can only be formed at high coverages by heating or flowing in an inert gas). These calculations shed new light on prior experimental studies leading to a more thorough understanding of BTX methylation reactions.

Concerted and sequential barriers tend to be within 20 kJ mol^{-1} of each other for the complete set of arene methylation reactions (from benzene to hexamethylbenzene), indicating that both mechanisms likely occur. Similarly, barriers for methylation by CH_3OH and CH_3OCH_3 are nearly identical, suggesting that either species can methylate arenes and that CH_3OH formed by CH_3OCH_3 reactions may itself react to form H_2O. Intrinsic methylation free energy barriers remain between 76 and 137 kJ mol^{-1} during repeated methylation of benzene to hexamethylbenzene suggesting that the number of methyl-substituents on the ring has no consistent trend with regards to raising or lowering activation barriers of methylation. Additionally, reaction free energies become less negative but generally remain low, suggesting that the formation of C_{10}–C_{12} species is unlikely kinetically limited during MTH reactions. This suggests that an aromatic compound, once formed during MTH, likely either desorbs from the zeolite as a light aromatic product (C_6–C_8) or forms an extensively methylated species, such as tetra-, penta-, or hexamethylbenzene. This extensively methylated arene will serve as a co-catalyst for olefin production and eventually lead to catalyst deactivation via the formation of polyaromatic species. Overall, this study provides mechanistic understanding of low-temperature BTX alkylations and gives insight into the dominant aromatic species present during MTH reactions while employing a novel method of identifying global minima and stable transition state structures within zeolite frameworks and revealing previously undescribed cooperativity between zeolite voids that enable the versatile chemistry of the MFI framework.

Associated Content

Supporting Information. Formulas and details of frequency calculations for enthalpy and free energy approximations, detailed images showing structures and reorientation schemes, derivations for arene methylation rate equations, and all activation and reaction enthalpies and entropies.

Acknowledgements. This work was funded by an ACS Petroleum Research Fund New Doctoral Investigation Award (57079-DNI5). Computational resources were provided by the Extreme Science and Engineering Discovery Environment (XSEDE),[78] which is supported by National Science Foundation grant number ACI-1548562 through allocation CTS160041. Additional computational resources were provided by University of Florida Research Computing.

References

(1) Jones, A. J.; Iglesia, E. Kinetic, spectroscopic, and theoretical assessment of associative and dissociative methanol dehydration routes in zeolites. *Angew. Chem. Int. Ed. Engl.* **2014**, *53*, 12177–12181 DOI: 10.1002/anie.201406823.

(2) Ghorbanpour, A.; Rimer, J. D.; Grabow, L. C. Computational Assessment of the Dominant Factors Governing the Mechanism of Methanol Dehydration over H-ZSM-5 with Heterogeneous Aluminum Distribution. *ACS Catal.* **2016**, *6*, 2287–2298 DOI: 10.1021/acscatal.5b02367.

(3) Sarazen, M. L.; Doskocil, E.; Iglesia, E. Effects of void environment and acid strength on alkene oligomerization selectivity. *ACS Catal.* **2016**, *6*, 7059–7070 DOI: 10.1021/acscatal.6b02128.

(4) Wang, S.; Agirrezabal-Telleria, I.; Bhan, A.; Simonetti, D.; Takanabe, K.; Iglesia, E. Catalytic routes to fuels from C1 and oxygenate molecules. *Faraday Discuss* **2017**, *197*, 9–39 DOI: 10.1039/c7fd00018a.

(5) Ilias, S.; Bhan, A. Mechanism of the catalytic conversion of methanol to hydrocarbons. *ACS Catal.* **2013**, *3*, 18–31 DOI: 10.1021/cs3006583.

(6) Van Speybroeck, V.; Van der Mynsbrugge, J.; Vandichel, M.; Hemelsoet, K.; Lesthaeghe, D.; Ghysels, A.; Marin, G. B.; Waroquier, M. First principle kinetic studies of zeolite-catalyzed methylation reactions. *J. Am. Chem. Soc.* **2011**, *133*, 888–899 DOI: 10.1021/ja1073992.

(7) Qi, L.; Wei, Y.; Xu, L.; Liu, Z. Reaction Behaviors and Kinetics during Induction Period of Methanol Conversion on HZSM-5 Zeolite. *ACS Catal.* **2015**, *5*, 3973–3982 DOI: 10.1021/acscatal.5b00654.

(8) Blaszkowski, S. R.; van Santen, R. A. Theoretical Study of C−C Bond Formation in the Methanol-to-Gasoline Process. *J. Am. Chem. Soc.* **1997**, *119*, 5020–5027 DOI: 10.1021/ja963530x.

(9) Wei, Z.; Chen, Y.-Y.; Li, J.; Guo, W.; Wang, S.; Dong, M.; Qin, Z.; Wang, J.; Jiao, H.; Fan, W. Stability and Reactivity of Intermediates of Methanol Related Reactions and C–C Bond Formation over H-ZSM-5 Acidic Catalyst: A Computational Analysis. *J. Phys. Chem. C* **2016**, *120*, 6075–6087 DOI: 10.1021/acs.jpcc.6b00211.

(10) Brogaard, R. Y.; Henry, R.; Schuurman, Y.; Medford, A. J.; Moses, P. G.; Beato, P.; Svelle, S.; Nørskov, J. K.; Olsbye, U. Methanol-to-hydrocarbons conversion: The alkene methylation pathway. *J. Catal.* **2014**, *314*, 159–169 DOI: 10.1016/j.jcat.2014.04.006.

(11) Svelle, S.; Kolboe, S.; Swang, O.; Olsbye, U. Methylation of alkenes and methylbenzenes by dimethyl ether or methanol on acidic zeolites. *J. Phys. Chem. B* **2005**, *109*, 12874–12878 DOI: 10.1021/jp051125z.

(12) Svelle, S.; Visur, M.; Olsbye, U.; Saepurahman; Bjørgen, M. Mechanistic Aspects of the Zeolite Catalyzed Methylation of Alkenes and Aromatics with Methanol: A Review. *Top. Catal.* **2011**, *54*, 897–906 DOI: 10.1007/s11244-011-9697-7.

(13) Svelle, S.; Arstad, B.; Kolboe, S.; Swang, O. A Theoretical Investigation of the Methylation of Alkenes with Methanol over Acidic Zeolites. *J. Phys. Chem. B* **2003**, *107*, 9281–9289 DOI: 10.1021/jp022201q.

(14) Hwang, A.; Prieto-Centurion, D.; Bhan, A. Isotopic tracer studies of methanol-to-olefins conversion over HSAPO-34: The role of the olefins-based catalytic cycle. *J. Catal.* **2016**, *337*, 52–56 DOI: 10.1016/j.jcat.2016.01.021.

(15) Lesthaeghe, D.; Van der Mynsbrugge, J.; Vandichel, M.; Waroquier, M.; Van Speybroeck, V. Full Theoretical Cycle for both Ethene and Propene Formation during Methanol-to-Olefin Conversion in H-ZSM-5. *ChemCatChem* **2011**, *3*, 208–212 DOI: 10.1002/cctc.201000286.

(16) Joshi, Y. V.; Bhan, A.; Thomson, K. T. DFT-Based Reaction Pathway Analysis of Hexadiene Cyclization via Carbenium Ion Intermediates: Mechanistic Study of Light Alkane Aromatization Catalysis. *J. Phys. Chem. B* **2004**, *108*, 971–980 DOI: 10.1021/jp036205m.

(17) Mullen, G. M.; Janik, M. J. Density Functional Theory Study of Alkane-Alkoxide Hydride Transfer in Zeolites. *ACS Catal.* **2011**, *1*, 105–115 DOI: 10.1021/cs1000619.

(18) Ilias, S.; Khare, R.; Malek, A.; Bhan, A. A descriptor for the relative propagation of the aromatic- and olefin-based cycles in methanol-to-hydrocarbons conversion on H-ZSM-5. *J. Catal.* **2013**, *303*, 135–140 DOI: 10.1016/j.jcat.2013.03.021.

(19) Lesthaeghe, D.; Horré, A.; Waroquier, M.; Marin, G. B.; Van Speybroeck, V. Theoretical insights on methylbenzene side-chain growth in ZSM-5 zeolites for methanol-to-olefin conversion. *Chem. Eur. J* **2009**, *15*, 10803–10808 DOI: 10.1002/chem.200901723.

(20) Arstad, B.; Nicholas, J. B.; Haw, J. F. Theoretical study of the methylbenzene side-chain hydrocarbon pool mechanism in methanol to olefin catalysis. *J. Am. Chem. Soc.* **2004**, *126*, 2991–3001 DOI: 10.1021/ja035923j.

(21) Wang, C.; Xu, J.; Qi, G.; Gong, Y.; Wang, W.; Gao, P.; Wang, Q.; Feng, N.; Liu, X.; Deng, F. Methylbenzene hydrocarbon pool in methanol-to-olefins conversion over zeolite H-ZSM-5. *J. Catal.* **2015**, *332*, 127–137 DOI: 10.1016/j.jcat.2015.10.001.

(22) Odedairo, T.; Balasamy, R. J.; Al-Khattaf, S. Toluene Disproportionation and Methylation over Zeolites TNU-9, SSZ-33, ZSM-5, and Mordenite Using Different Reactor Systems. *Ind Eng Chem Res* **2011**, *50*, 3169–3183 DOI: 10.1021/ie1018904.

(23) Beschmann, K.; Riekert, L. Isomerization of Xylene and Methylation of Toluene on Zeolite H-ZSM-5. Compound Kinetics and Selectivity. *J. Catal.* **1993**, *141*, 548–565 DOI: 10.1006/jcat.1993.1163.

(24) Cha, S. H.; Hong, S. B. Reaction intermediates and mechanism of the zeolite-catalyzed transalkylation of 1,2,4-trimethylbenzene with toluene. *J. Catal.* **2018**, *357*, 1–11 DOI: 10.1016/j.jcat.2017.10.015.

(25) Vos, A. M.; Rozanska, X.; Schoonheydt, R. A.; van Santen, R. A.; Hutschka, F.; Hafner, J. A theoretical study of the alkylation reaction of toluene with methanol catalyzed by acidic mordenite. *J. Am. Chem. Soc.* **2001**, *123*, 2799–2809 DOI: 10.1021/ja001981i.

(26) Wen, Z.; Yang, D.; He, X.; Li, Y.; Zhu, X. Methylation of benzene with methanol over HZSM-11 and HZSM-5: A density functional theory study. *J. Mol. Catal. A: Chem* **2016**, *424*, 351–357 DOI: 10.1016/j.molcata.2016.07.051.

(27) Saepurahman; Visur, M.; Olsbye, U.; Bjørgen, M.; Svelle, S. In Situ FT-IR Mechanistic Investigations of the Zeolite Catalyzed Methylation of Benzene with Methanol: H-ZSM-5 versus H-beta. *Top. Catal.* **2011**, *54*, 1293–1301 DOI: 10.1007/s11244-011-9751-5.

(28) Hill, I.; Malek, A.; Bhan, A. Kinetics and Mechanism of Benzene, Toluene, and Xylene Methylation over H-MFI. *ACS Catal.* **2013**, *3*, 1992–2001 DOI: 10.1021/cs400377b.

(29) Hill, I. M.; Hashimi, S. A.; Bhan, A. Kinetics and mechanism of olefin methylation reactions on zeolites. *J. Catal.* **2012**, *285*, 115–123 DOI: 10.1016/j.jcat.2011.09.018.

(30) Svelle, S.; Ronning, P.; Olsbye, U.; Kolboe, S. Kinetic studies of zeolite-catalyzed methylation reactions. Part 2. Co-reaction of [12C]propene or [12C]n-butene and [13C]methanol. *J. Catal.* **2005**, *234*, 385–400 DOI: 10.1016/j.jcat.2005.06.028.

(31) Svelle, S.; Rønning, P. O.; Kolboe, S. Kinetic studies of zeolite-catalyzed methylation reactions1. Coreaction of [12C]ethene and [13C]methanol. *J. Catal.* **2004**, *224*, 115–123 DOI: 10.1016/j.jcat.2004.02.022.

(32) Vos, A. M.; Nulens, K. H. L.; De Proft, F.; Schoonheydt, R. A.; Geerlings, P. Reactivity descriptors and rate constants for electrophilic aromatic substitution: acid zeolite catalyzed methylation of benzene and toluene. *J. Phys. Chem. B* **2002**, *106*, 2026–2034 DOI: 10.1021/jp014015a.

(33) Moors, S. L. C.; De Wispelaere, K.; Van der Mynsbrugge, J.; Waroquier, M.; Van Speybroeck, V. Molecular Dynamics Kinetic Study on the Zeolite-Catalyzed Benzene Methylation in ZSM-5. *ACS Catal.* **2013**, *3*, 2556–2567 DOI: 10.1021/cs400706e.

(34) Gomes, J.; Zimmerman, P. M.; Head-Gordon, M.; Bell, A. T. Accurate Prediction of Hydrocarbon Interactions with Zeolites Utilizing Improved Exchange-Correlation Functionals and QM/MM Methods: Benchmark Calculations of Adsorption Enthalpies and Application to Ethene Methylation by Methanol. *J. Phys. Chem. C* **2012**, *116*, 15406–15414 DOI: 10.1021/jp303321s.

(35) De Wispelaere, K.; Martínez-Espín, J. S.; Hoffmann, M. J.; Svelle, S.; Olsbye, U.; Bligaard, T. Understanding zeolite-catalyzed benzene methylation reactions by methanol and dimethyl ether at operating conditions from first principle microkinetic modeling and experiments. *Catal. Today* **2018**, *312*, 35–43 DOI: 10.1016/j.cattod.2018.02.042.

(36) Martinez-Espin, J. S.; Mortén, M.; Janssens, T. V. W.; Svelle, S.; Beato, P.; Olsbye, U. New insights into catalyst deactivation and product distribution of zeolites in the methanol-to-hydrocarbons (MTH) reaction with methanol and dimethyl ether feeds. *Catal. Sci. Technol.* **2017**, *7*, 2700–2716 DOI: 10.1039/C7CY00129K.

(37) Martinez-Espin, J. S.; De Wispelaere, K.; Westgård Erichsen, M.; Svelle, S.; Janssens, T. V. W.; Van Speybroeck, V.; Beato, P.; Olsbye, U. Benzene co-reaction with methanol and dimethyl ether over zeolite and zeotype catalysts: Evidence of parallel reaction paths to toluene and diphenylmethane. *J. Catal.* **2017**, *349*, 136–148 DOI: 10.1016/j.jcat.2017.03.007.

(38) Arstad, B.; Kolboe, S.; Swang, O. A theoretical investigation on the methylation of methylbenzenes on zeolites. *J. Phys. Chem. B* **2002**, *106*, 12722–12726 DOI: 10.1021/jp020851o.

(39) Kresse, G.; Hafner, J. *Ab initio* molecular dynamics for liquid metals. *Phys. Rev. B* **1993**, *47*, 558–561 DOI: 10.1103/PhysRevB.47.558.

(40) Kresse, G.; Hafner, J. Ab initio molecular-dynamics simulation of the liquid-metal-amorphous-semiconductor transition in germanium. *Phys. Rev. B, Condens. Matter* **1994**, *49*, 14251–14269 DOI: 10.1103/PhysRevB.49.14251.

(41) Kresse, G.; Furthmüller, J. Efficient iterative schemes for ab initio total-energy calculations using a plane-wave basis set. *Phys. Rev. B, Condens. Matter* **1996**, *54*, 11169–11186.

(42) Kresse, G.; Furthmüller, J. Efficiency of ab-initio total energy calculations for metals and semiconductors using a plane-wave basis set. *Comp. Mater. Sci.* **1996**, *6*, 15–50 DOI: 10.1016/0927-0256(96)00008-0.

(43) Blöchl, P. E. Projector augmented-wave method. *Phys. Rev. B, Condens. Matter* **1994**, *50*, 17953–17979.

(44) Kresse, G.; Joubert, D. From ultrasoft pseudopotentials to the projector augmented-wave method. *Phys. Rev. B* **1999**, *59*, 1758–1775 DOI: 10.1103/PhysRevB.59.1758.

(45) Perdew, J. P.; Burke, K.; Ernzerhof, M. Generalized gradient approximation made simple. *Phys. Rev. Lett.* **1996**, *77*, 3865–3868 DOI: 10.1103/PhysRevLett.77.3865.

(46) Zhang, Y.; Yang, W. Comment on "Generalized Gradient Approximation Made Simple. *Phys. Rev. Lett.* **1998**, *80*, 890–890 DOI: 10.1103/PhysRevLett.80.890.

(47) Hammer, B.; Hansen, L. B.; Nørskov, J. K. Improved adsorption energetics within density-functional theory using revised Perdew-Burke-Ernzerhof functionals. *Phys. Rev. B* **1999**, *59*, 7413–7421 DOI: 10.1103/PhysRevB.59.7413.

(48) Grimme, S.; Ehrlich, S.; Goerigk, L. Effect of the damping function in dispersion corrected density functional theory. *J. Comput. Chem.* **2011**, *32*, 1456–1465 DOI: 10.1002/jcc.21759.

(49) Schröder, H.; Creon, A.; Schwabe, T. Reformulation of the D3(Becke-Johnson) Dispersion Correction without Resorting to Higher than C_6 Dispersion Coefficients. *J. Chem. Theory Comput.* **2015**, *11*, 3163–3170 DOI: 10.1021/acs.jctc.5b00400.

(50) Grimme, S.; Antony, J.; Ehrlich, S.; Krieg, H. A consistent and accurate ab initio parametrization of density functional dispersion correction (DFT-D) for the 94 elements H-Pu. *J. Chem. Phys.* **2010**, *132*, 154104 DOI: 10.1063/1.3382344.

(51) Monkhorst, H. J.; Pack, J. D. Special points for Brillouin-zone integrations. *Phys. Rev. B* **1976**, *13*, 5188–5192 DOI: 10.1103/PhysRevB.13.5188.

(52) Baerlocher, C.; McCusker, L. B. Database of Zeolite Structures: http://www.iza-structure.org/databases. **2013**.

(53) Hoffman, A.; DeLuca, M.; David Hibbitts. Restructuring of MFI Framework Zeolite Models and their Associated Artifacts in DFT Calculations.

(54) Jónsson, H.; Mills, G.; Jacobsen, K. W. Nudged elastic band method for finding minimum energy paths of transitions. In *Classical and Quantum Dynamics in Condensed Phase Simulations*; Berne, B. J.; Ciccotti, G.; Coker, D. F., Eds.; World Scientific, 1998; pp. 385–404.

(55) Henkelman, G.; Jónsson, H. Improved tangent estimate in the nudged elastic band method for finding minimum energy paths and saddle points. *J. Chem. Phys.* **2000**, *113*, 9978–9985 DOI: 10.1063/1.1323224.

(56) Henkelman, G.; Jónsson, H. A dimer method for finding saddle points on high dimensional potential surfaces using only first derivatives. *J. Chem. Phys.* **1999**, *111*, 7010–7022 DOI: 10.1063/1.480097.

(57) Herrmann, S.; Iglesia, E. Elementary steps in acetone condensation reactions catalyzed by aluminosilicates with diverse void structures. *J. Catal.* **2017**, *346*, 134–153 DOI: 10.1016/j.jcat.2016.12.011.

(58) Zhi, Y.; Shi, H.; Mu, L.; Liu, Y.; Mei, D.; Camaioni, D. M.; Lercher, J. A. Dehydration Pathways of 1-Propanol on HZSM-5 in the Presence and Absence of Water. *J. Am. Chem. Soc.* **2015**, *137*, 15781–15794 DOI: 10.1021/jacs.5b09107.

(59) Nystrom, S.; Hoffman, A.; Hibbitts, D. Tuning Brønsted acid strength by altering site proximity in CHA framework zeolites. *ACS Catal.* **2018**, *8*, 7842–7860 DOI: 10.1021/acscatal.8b02049.

(60) Flaherty, D. W.; Iglesia, E. Transition-state enthalpy and entropy effects on reactivity and selectivity in hydrogenolysis of n-alkanes. *J. Am. Chem. Soc.* **2013**, *135*, 18586–18599 DOI: 10.1021/ja4093743.

(61) Flaherty, D. W.; Hibbitts, D. D.; Gürbüz, E. I.; Iglesia, E. Theoretical and kinetic assessment of the mechanism of ethane hydrogenolysis on metal surfaces saturated with chemisorbed hydrogen. *J. Catal.* **2014**, *311*, 350–356 DOI: 10.1016/j.jcat.2013.11.026.

(62) Flaherty, D. W.; Hibbitts, D. D.; Iglesia, E. Metal-catalyzed C-C bond cleavage in alkanes: effects of methyl substitution on transition-state structures and stability. *J. Am. Chem. Soc.* **2014**, *136*, 9664–9676 DOI: 10.1021/ja5037429.

(63) Vinek, H.; Lercher, J. A. Production and reactions of xylenes over H-ZSM5. *Journal of Molecular Catalysis* **1991**, *64*, 23–39 DOI: 10.1016/0304-5102(91)85125-L.

(64) Chirico, R. D.; Steele, W. V. Thermodynamic Equilibria in Xylene Isomerization. 5. Xylene Isomerization Equilibria from Thermodynamic Studies and Reconciliation of Calculated and Experimental Product Distributions†. *J. Chem. Eng. Data* **1997**, *42*, 784–790 DOI: 10.1021/je970030q.

(65) Gobin, O. C.; Reitmeier, S. J.; Jentys, A.; Lercher, J. A. Diffusion pathways of benzene, toluene and p-xylene in MFI. *Micropor. Mesopor. Mat.* **2009**, *125*, 3–10 DOI: 10.1016/j.micromeso.2009.01.025.

(66) Pope, C. G. Sorption of benzene, toluene and p-xylene on ZSM-5. *J. Phys. Chem.* **1984**, *88*, 6312–6313 DOI: 10.1021/j150669a051.

(67) Kaeding, W. Selective alkylation of toluene with methanol to produce para-Xylene. *J. Catal.* **1981**, *67*, 159–174 DOI: 10.1016/0021-9517(81)90269-4.

(68) Kaeding, W. Shape-selective reactions with zeolite catalysts II. Selective disproportionation of toluene to produce benzene and p-Xylene. *J. Catal.* **1981**, *69*, 392–398 DOI: 10.1016/0021-9517(81)90174-3.

(69) Ahn, J. H.; Kolvenbach, R.; Gutiérrez, O. Y.; Al-Khattaf, S. S.; Jentys, A.; Lercher, J. A. Tailoring p-xylene selectivity in toluene methylation on medium pore-size zeolites. *Micropor. Mesopor. Mat.* **2015**, *210*, 52–59 DOI: 10.1016/j.micromeso.2015.02.018.

(70) Ilias, S.; Bhan, A. The mechanism of aromatic dealkylation in methanol-to-hydrocarbons conversion on H-ZSM-5: What are the aromatic precursors to light olefins? *J. Catal.* **2014**, *311*, 6–16 DOI: 10.1016/j.jcat.2013.11.003.

(71) Wang, C.-M.; Wang, Y.-D.; Liu, H.-X.; Yang, G.; Du, Y.-J.; Xie, Z.-K. Aromatic-based hydrocarbon pool mechanism for methanol-to-olefins conversion in H-SAPO-18: A van der Waals density functional study. *Chinese Journal of Catalysis* **2015**, *36*, 1573–1579 DOI: 10.1016/S1872-2067(15)60891-9.

(72) Dessau, R. On the mechanism of methanol conversion to hydrocarbons over HZSM-5. *J. Catal.* **1982**, *78*, 136–141 DOI: 10.1016/0021-9517(82)90292-5.

(73) Ilias, S.; Bhan, A. Tuning the selectivity of methanol-to-hydrocarbons conversion on H-ZSM-5 by co-processing olefin or aromatic compounds. *J. Catal.* **2012**, *290*, 186–192 DOI: 10.1016/j.jcat.2012.03.016.

(74) Wang, C.-M.; Wang, Y.-D.; Xie, Z.-K. Verification of the dual cycle mechanism for methanol-to-olefin conversion in HSAPO-34: a methylbenzene-based cycle from DFT calculations. *Catal. Sci. Technol.* **2014**, *4*, 2631–2638 DOI: 10.1039/C4CY00262H.

(75) Mores, D.; Kornatowski, J.; Olsbye, U.; Weckhuysen, B. M. Coke formation during the methanol-to-olefin conversion: in situ microspectroscopy on individual H-ZSM-5 crystals with different Brønsted acidity. *Chem. Eur. J* **2011**, *17*, 2874–2884 DOI: 10.1002/chem.201002624.

(76) Rojo-Gama, D.; Signorile, M.; Bonino, F.; Bordiga, S.; Olsbye, U.; Lillerud, K. P.; Beato, P.; Svelle, S. Structure–deactivation relationships in zeolites during the methanol–to-hydrocarbons reaction: Complementary assessments of the coke content. *J. Catal.* **2017**, *351*, 33–48 DOI: 10.1016/j.jcat.2017.04.015.

(77) Bjørgen, M.; Olsbye, U.; Kolboe, S. Coke precursor formation and zeolite deactivation: mechanistic insights from hexamethylbenzene conversion. *J. Catal.* **2003**, *215*, 30–44 DOI: 10.1016/S0021-9517(02)00050-7.

(78) Towns, J.; Cockerill, T.; Dahan, M.; Foster, I.; Gaither, K.; Grimshaw, A.; Hazlewood, V.; Lathrop, S.; Lifka, D.; Peterson, G. D.; et al. XSEDE: accelerating scientific discovery. *Comput Sci Eng* **2014**, *16*, 62–74 DOI: 10.1109/MCSE.2014.80.